Evaluation of ozone total column measurements by the Ozone Monitoring Instrument using a data assimilation system

S. Migliorini,[1] R. Brugge,[1] A. O'Neill,[1] M. Dobber,[2] V. Fioletov,[3] P. Levelt,[2] and R. McPeters[4]

Received 11 April 2007; revised 8 January 2008; accepted 6 February 2008; published 10 May 2008.

[1] On 15 July 2004, the Ozone Monitoring Instrument (OMI) on board the EOS Aura mission was launched. One of OMI's priorities is to continue the record of high spatial resolution ozone total column measurements provided by the various Total Ozone Mapping Spectrometer (TOMS) instruments since 1978. To this end, it is essential to estimate the errors affecting OMI ozone total column measurements and to see whether the actual accuracy is consistent with estimated values before launch. In this paper, data assimilation techniques are used to create a large comparison data set composed of ozone analyses resulting from assimilation of standard meteorological observations and ozone retrievals (independent of OMI measurements) into a numerical weather prediction model. This data set provides excellent global coverage and temporal resolution, not limited by the spatial and temporal distribution of other satellite or ground based information. The accuracy of the analyses is evaluated against ozone total column retrievals from Brewer measurements, while the assimilated ozone data set is compared to ozone predictions made using the ECMWF model, to check for the presence of bias. The OMI ozone column measurements considered here are obtained with the TOMS-V8 total ozone algorithm and denoted as OMTO3 columns. They are compared with simulated OMI ozone columns, i.e., the quantities that the TOMS-V8 algorithm would retrieve in the case when the atmospheric ozone profile at a specific location and time is equal to the one prescribed by the analysis. In this way, the comparison is statistically robust even when data acquired during a relatively short temporal interval or over a relatively small geographical area only is considered. A discussion of relevant error sources (including systematic components), vertical resolution, and contributions from prior information is provided. Special attention is given to determining the importance of representativeness errors. Our results show a solar zenith angle (SZA) dependence of the bias between measured and simulated OMI columns. This is believed to be due to moderate nonlinearity of the observation forward model and its effects on our definition of simulated OMI columns at high SZA. In view of these findings the final results of the intercomparison methodology used in this paper are obtained from OMI ozone columns retrieved using the basic implementation of the TOMS-V8 algorithm applied to measurements taken at SZA not exceeding 70°. Intercomparison results between measured and simulated OMI ozone columns at SZA less than 70° show a relative bias of $-3.2 \pm 3.1\%$ and a root-mean-square error of $4.5 \pm 1.5\%$. The resulting bias is consistent with available estimates of the bias of OMTO3 columns with respect to SBUV/2 between 60°S and 60°N, as well as with respect to global Dobson data and Brewer measurements between 30°N and 60°N.

Citation: Migliorini, S., R. Brugge, A. O'Neill, M. Dobber, V. Fioletov, P. Levelt, and R. McPeters (2008), Evaluation of ozone total column measurements by the Ozone Monitoring Instrument using a data assimilation system, *J. Geophys. Res.*, *113*, D15S21, doi:10.1029/2007JD008779.

1. Introduction

[2] Along with the other instruments on the EOS-Aura platform [*Schoeberl et al.*, 2006], the Ozone Monitoring Instrument (OMI) [*Levelt et al.*, 2006a] contributes to the scientific goals of the Aura mission, which include an assessment of the expected recovery of the ozone layer. One of the objectives of OMI [*Levelt et al.*, 2006b] is to continue the total column ozone measurements provided by

[1]Data Assimilation Research Centre, University of Reading, Reading, UK.
[2]Royal Netherlands Meteorological Institute, De Bilt, Netherlands.
[3]Environment Canada, Toronto, Ontario, Canada.
[4]NASA Goddard Space Flight Center, Greenbelt, Maryland, USA.

0148-0227/08/2007JD008779$09.00

the Solar Backscatter Ultraviolet (SBUV) [e.g., *Hilsenrath et al.*, 1995] and Total Ozone Mapping Spectrometer (TOMS) instruments [e.g., *Jaross et al.*, 1995]. It is also to provide an improved spatial resolution. The TOMS Version 8 algorithm [*Bhartia and Wellemeyer*, 2002] was applied to reprocess the data from the Nimbus-7 and Earth Probe spacecrafts from 1 November 1978 to 6 May 1993 and from 25 July 1996 to 31 December 2005, respectively, and Nimbus-7 SBUV data between 1978 and 1990. Therefore, this algorithm was also used for deriving total column ozone data from OMI measurements.

[3] In order to achieve the OMI objectives it is hence essential to estimate the accuracy of the ozone data retrieved from OMI measurements. For this purpose, the ozone retrievals from OMI need to be compared with independent and coincident ozone measurements from other instruments, both in situ and from remote sounding. The scope for validation is limited by the availability of a suitable comparison data set, in particular when in situ measurements such as ozone sondes or aircraft data are considered. Remote sounding instruments give a better temporal and spatial coverage, although it can still be challenging to find a sufficient number of coincidences for a statistically significant intercomparison. Also, remote sounders provide typically an estimate of an atmospheric ozone profile that is smoothed by means of a set of averaging kernel functions and includes some prior information to constrain the inverse problem. Finally, retrieval errors are correlated between different altitudes. This implies that in order to compare OMI retrievals with estimates from independent remote sounding instruments, the averaging kernels and error covariance matrix of the different retrievals are needed [*Rodgers and Connor*, 2003]. This can make the comparison a rather challenging process.

[4] A complementary approach to the one discussed above is to perform validation by first assimilating independent measurements into a suitable model of the atmosphere. The resulting analyses are then interpolated to the location and time of the measurements by the instrument to be validated. These measurements are then compared to the interpolated analyses [e.g., *Stajner et al.*, 2004]. Each analysis will describe the resulting field (e.g., ozone) after assimilation of both standard meteorological observations (e.g., sondes, aircraft, satellite radiances) and of data that are directly related to the considered field (e.g., satellite radiances sensitive to ozone from independent instruments). With this approach it is possible to increase the number of coincidences significantly: the availability of a gridded field (the analysis) at various assimilation times allow us to perform comparisons over the entire region covered by the satellite measurements, i.e., the whole globe in the case of polar orbiting satellites. This can also help to investigate systematic errors that may affect the measurements over specific regions or that are dependent on the time of day when the measurement is taken. Note that analyses provide only an indirect estimate of the field of interest. As in the case of retrievals, analyses are characterized by a set of averaging kernels, which are represented by the rows of the matrix given formally by the product of the Kalman gain times the linearized observation operator. A limitation on the use of analyses for validation is given by the fact that a variational data assimilation system (DAS), used by most operational meteorological centres for producing atmospheric analyses, generally does not provide the analysis averaging kernels nor the analysis error covariance matrix on a routine basis.

[5] The aim of this paper is to use data assimilation techniques for validating ozone total columns retrieved from OMI measurements by means of the TOMS Version 8 algorithm. Ozone analyses were used to create simulated OMI ozone columns. These simulated OMI columns represent the quantities that the TOMS-V8 algorithm would retrieve in the case when the atmospheric ozone profile at a specific location and time is equal to the one prescribed by the analysis. Each simulated OMI column was compared to an actual OMI measurement that complied with the chosen coincidence criterion. Care was taken in detailing all known error sources in the comparison. These include errors due to insufficient resolution for simulating OMI measurements properly or representativeness errors. Results quantifying the level of agreement between OMI ozone data and the ozone analyses are provided. Implications arising from the lack of knowledge about the analysis averaging kernels and the analysis error covariance matrix are discussed in section 3. Our study focuses on OMI measurements taken during a relatively short period of time (about 2.5 months) in order to keep our computational costs within the available resources. This should be borne in mind when making use of our results.

2. Description of the Comparison Data Set

[6] In this section, the case study and the data set considered in this paper for evaluating OMI ozone columns against ozone analyses are described. The 2005 ozone hole, which reached a maximum area (defined as the area where the ozone total column is less than 220 DU) of about 27 Mkm^2 on 19 September, ranks as the third largest on record. Also, minimum temperatures inside the stratospheric vortex were, in early September, near the lowest recorded since 1979 [*World Meteorological Organization*, 2006]. The high degree of variability in ozone column values, especially around the vortex, makes this period interesting for testing the performance of an ozone-sensitive satellite instrument.

[7] An updated version of the 3D-Var data assimilation scheme as conceived for ERA-40, a reanalysis of meteorological observations from September 1957 to August 2002 produced by the European Centre for Medium-Range Weather Forecasts (ECMWF), was used to carry out a data assimilation experiment during our case study, defined between 12 August 2005 0000 UTC and 31 October 2005 1800 UTC. A model configuration with a T159L60 resolution and top model level at 0.1 hPa was chosen, characterized by a vertical resolution of about 1.5 km over much of the stratosphere. A 6-h assimilation period was considered, with a ''first-guess at the appropriate time'' approach: observations within a time window centered at the analysis time were compared with model forecasts valid nearest the actual observation time, rather than at the analysis time [*Uppala et al.*, 2005].

2.1. Ozone Analyses

[8] The assimilation data set in our experiment is composed of operational observations (e.g., sondes, aircraft,

satellite radiances sensitive to atmospheric temperature) plus ozone observations from SBUV/2 on board the NOAA-16 platform and from SCIAMACHY flying on the ESA's Envisat mission. In addition to these ozone measurements, which are routinely assimilated at ECMWF, it was decided to constrain the model ozone field further by assimilating ozone profiles from the Microwave Limb Sounder (MLS) [*Waters et al.*, 2006] on the NASA's Aura satellite. The ozone analyses resulting from the assimilation of the data set described above were used to create simulated OMI ozone columns for comparison to the actual OMI measurements over the period of the assimilation experiment.

[9] SBUV/2 ozone data are processed using the Version 6 retrieval algorithm [*Bhartia et al.*, 1996] with an included out of band response correction as well as an improved calibration (see http://www.orbit.nesdis.noaa.gov/smcd/spb/ozone/sbuv-16.html). In the ECMWF DAS, the original 12 layers from the standard data product are combined into five layers (between 0.12 hPa and 15.83 hPa) plus an extra layer below 15.83 hPa which contains the difference between the ozone total column and the partial column above 15.83 hPa. Assimilated SCIAMACHY data comprise ozone total columns retrieved by using the "Total Ozone retrieval scheme for SCIAMACHY based on the OMI DOAS algorithm" (TOSOMI), described in the work of *Eskes et al.* [2005]. The MLS data were retrieved using algorithm version 1.5 [*Livesey et al.*, 2006]. The standard products have 46 retrieval levels from 1000 hPa to 0.001 hPa but are recommended for use only in the range 215–0.46 hPa. For the assimilation experiment, the data given at 21 pressure levels between 215 and 0.1 hPa were converted into ozone partial columns over 20 layers. Early MLS validation results [*Froidevaux et al.*, 2006] show that MLS ozone profiles agree to about the 5–10% level with stratospheric profiles from the Stratospheric Aerosol and Gas Experiment II (SAGE II), the Halogen Occultation Experiment (HALOE), the Polar Ozone and Aerosol Measurement III (POAM III), and the Atmospheric Chemistry Experiment (ACE).

[10] General details on ozone assimilation at ECMWF can be found in the work of *Dethof and Hólm* [2004]. In particular, the background error covariance matrix for ozone consists of globally uniform error correlations from an ensemble of forecast differences and of spatially varying variances. In the forecasting model, the parametrization of source and sink terms in the prognostic equation for ozone is an updated version of *Cariolle and Déqué* [1986] and accounts for both photochemistry and heterogeneous chemistry. The photochemistry part depends linearly on the local ozone mixing ratio, the temperature, and the partial ozone column above the considered atmospheric level. The latter is activated only for temperatures below 195 K.

[11] Before using ECMWF ozone analyses for intercomparison with OMI data, it is necessary to assess whether they agree with independent data. *Dethof and Hólm* [2004] present some intercomparison results with ground-based total ozone observations, which are relevant to our work despite the differences in the assimilated data set. They conclude that total ozone analyses are in good agreement with independent data even without ozone assimilation, with the exception of the ozone hole at the South Pole being too deep between 1957 and 1972 (when no satellite data was available) and not deep enough between 1973 and 1978 (when no ozone sensitive satellite data was available). However, these problems disappear when ozone data from SBUV and TOMS are assimilated. While these results are encouraging, a quantitative evaluation of the analyses containing information from the ozone data specifically used for our assimilation experiment is needed. This is discussed in section 4.1.

[12] Another way to check for the possible presence of biases in the assimilated ozone data set is through monitoring of the temporal sequence of innovations, i.e., observation-minus-forecast residuals. As a matter of fact, a bias in the innovation sequence of a given observation of a parameter of interest (in our case the ozone field) denotes a bias in the forecasts and/or in the assimilated observations [e.g., *Dee and da Silva*, 1998, section 3a]. When, for example, biased observations are assimilated by means of a standard assimilation algorithm (which assumes both forecasts and observations being unbiased), the resulting analyses are also biased. These analyses then represent a less accurate quantity to be used for evaluation of independent observations. In section 4.2, the ozone innovation sequences for our data assimilation experiment will be discussed.

2.2. OMI Ozone Data Set

[13] OMI is a Dutch-Finnish instrument on board the NASA's EOS-Aura satellite flying on a sun-synchronous polar orbit and launched on 15 July 2004. OMI is a nadir-viewing, near-ultraviolet and visible spectrometer measuring solar radiation reflected by the Earth in the spectral range between 270 and 500 nm. The instrument is composed of two optical channels: one in the ultraviolet range between 270 and 383 nm and the other in the visible between 349 and 500 nm. The ultraviolet channel is subdivided in the UV1 subchannel, between 270 and 311 nm with a ground pixel size at nadir of 13×8 km^2 (along x across track), and the UV2 subchannel, between 307 and 383 nm with a ground pixel size at nadir of 13×24 km^2. The visible channel ground pixel size is the same as for UV2. The spectral resolution is about 0.5 nm and the field of view corresponds to a 2600 km swath width allowing for daily global coverage [*Levelt et al.*, 2006a].

[14] The OMI ozone total column data product discussed in this paper was obtained using the TOMS-V8 ozone total column algorithm [*Bhartia and Wellemeyer*, 2002] with the software version 0.9.45 and referred to as OMTO3. The TOMS Version 8 algorithm makes use of only one to two pairs of wavelengths in the UV2 subchannel depending on the solar zenith angle (SZA): 317.5 and 331.2 nm for SZA up to 70° and also the second pair consisting of 312.5 and 331.2 nm for larger SZA. The OMTO3 data product is characterized by a pixel size at nadir of 13×24 km^2.

[15] According to *Ziemke et al.* [2006], who reference a personal communication from G. Labow, OMTO3 measurements have been validated by comparing them with ground-based Dobson and NOAA-16 SBUV/2 data. These comparisons show that OMTO3 data are around 0.5% higher than the Dobson measurements and within 1% with respect to SBUV/2 for latitudes between −60° and 60°. Also, results from a comparison for the period between August 2004 and September 2006 [*Balis et al.*, 2007]

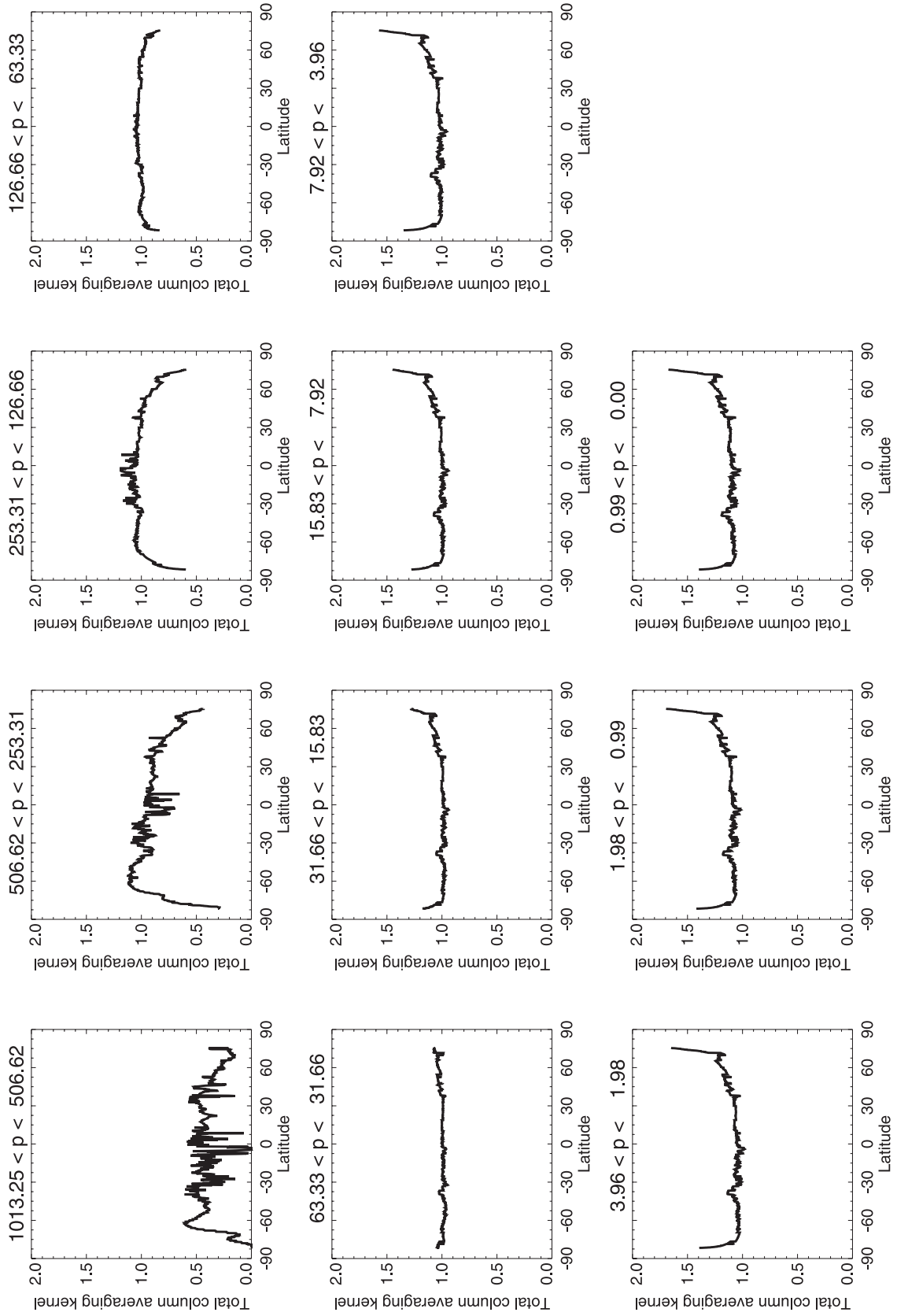
1013.25 < p < 506.62
506.62 < p < 253.31
253.31 < p < 126.66
126.66 < p < 63.33
63.33 < p < 31.66
31.66 < p < 15.83
15.83 < p < 7.92
7.92 < p < 3.96
3.96 < p < 1.98
1.98 < p < 0.99
0.99 < p < 0.00
Total column averaging kernel
Latitude
0.0
0.5
1.0
1.5
2.0
-90
-60
-30
0
30
60
90

Figure 1

show that the global average of the difference between OMTO3 retrievals and Dobson data is 0.57 ± 3.50%, while the average difference between OMTO3 retrievals and data from Brewer instruments (mainly located between 30° N and 60° N) is −0.03 ± 3.50%.

[16] The OMTO3 algorithm [*Bhartia and Wellemeyer*, 2002] relies on the fact that the radiance measured by a satellite instrument at wavelengths longer than 310 nm is mostly sensitive to ozone total column and only weakly sensitive to the ozone profile shape. Given the need for a high accuracy, the radiative transfer model used to calculate the upwelling radiance includes a correction to account for contributions from different profiles with the same integrated column. The appropriate ozone profile is selected from a data set of 1512 profiles that vary with latitude, month, and ozone total column generated using ozonesonde and satellite data. These profiles can also be interpreted as a set of a priori constraints imposed on the retrieval by the OMTO3 algorithm. Note that since the ozone profiles provide a higher-order correction to the total column sensitivity, the profiles considered by the algorithm are actually partial columns integrated over 10 atmospheric layers with equal thicknesses of log(2) in log-pressure from 1 atm (1013.25 hPa) to 2^{-10} atm, plus a top layer which includes the remainder of the upper atmosphere.

[17] In order to understand the general relationship between ozone total column measurements and ozone profiles, let us define the true ozone total column $\Omega = \mathbf{g}^T \mathbf{x}$ as the result of the scalar product between $\mathbf{x}$, the true ozone vertical profile, and $\mathbf{g}$, an integration operator. A remote sounding instrument provides an estimate $\hat{\mathbf{x}}$ of the ozone profile that can be expressed as [*Rodgers*, 2000, section 3.1]

$$\hat{\mathbf{x}} = \mathbf{x}_a + \mathbf{A}(\mathbf{x} - \mathbf{x}_a) + \boldsymbol{\epsilon}_x \tag{1}$$

where $\mathbf{A}$ is the ozone profile averaging kernel matrix calculated by the retrieval method, $\mathbf{x}_a$ is the a priori ozone profile selected as a constraint and $\boldsymbol{\epsilon}_x$ is the retrieval error. For the expression in equation (1) to be valid, the forward model that calculates the logarithm of the radiance emerging from the top of the atmosphere needs to be linear to better than the measurement error within the region of the state space, centered on the retrieval, where the true state (e.g., the true atmospheric ozone or temperature profile) may lie [*Rodgers*, 2000, section 5.5]. In this case the estimated column $\hat{\Omega}$ can then be expressed as

$$\hat{\Omega} = \Omega_a + \mathbf{a}^T(\mathbf{x} - \mathbf{x}_a) + \epsilon_\Omega \tag{2}$$

where $\Omega_a = \mathbf{g}^T\mathbf{x}_a$ is the a priori total column, $\epsilon_\Omega = \mathbf{g}^T\boldsymbol{\epsilon}_x$, and $\mathbf{a}^T = \mathbf{g}^T\mathbf{A}$ is the total column averaging kernel. This means that only when $\mathbf{A} \equiv \mathbf{I}$ can the total column be regarded as a direct estimate of Ω, or $\hat{\Omega} = \Omega + \epsilon_\Omega$, with full vertical resolution and no use of prior information. When a profile of partial columns is considered, each element of $\mathbf{a}$ represents the sensitivity of the total column estimation with respect to perturbations of each partial column of ozone actually present in the atmosphere (i.e., of each element of the true state $\mathbf{x}$). In this case $\mathbf{g}$ is simply the identity vector and $\mathbf{a}$ can be interpreted as a layer efficiency factor vector, with components given by the sum of the columns of $\mathbf{A}$.

[18] In the case of OMTO3 data, even though detailed calculations [*Bhartia and Wellemeyer*, 2002] show that the layer efficiency factors are close to the ideal value of one (when $\mathbf{g}$ is the identity vector and $\mathbf{A} \equiv \mathbf{I}$ then $\mathbf{a}$ is also the identity vector.) for most vertical layers, they can have variations for high solar zenith angles and below about 5 km. An example of this is shown in Figure 1 where the layer efficiency factors for nadir pixels on 15 October 2005 are presented as a function of latitude. Hence, according to equation (2), OMTO3 data will provide an estimate of the ozone total column with finite resolution and contributions from prior information.

[19] The 14 to 15 OMTO3 data files per day, with one file per orbit, are provided by the Goddard Earth Sciences Distributed Active Archive Center. Each file includes data referring to the sun-lit section of an OMI orbit. Along with an estimate of ozone total columns, each OMTO3 data file contains the total column averaging kernel vectors and a priori profiles of partial columns appropriate for each total column. All these quantities will be used for intercomparison, as explained in the next section.

3. Intercomparison Methodology

[20] Here we detail how each OMI ozone column within our data set is compared to a given ozone analysis, with a discussion of the error sources, both random and systematic, and the methodology for estimating key statistical figures characterizing the comparison. First, a suitable OMTO3 measurement, screened for solar zenith angle higher than 84° surface glint, and SO_2 contamination, needs to be related to an ECMWF ozone analysis profile according to a coincidence criterion for the duration of the assimilation experiment to form a colocated data set for intercomparison. Given the relatively high data availability, a rather strict criterion was applied: only OMI measurements taken within 1 h from an available analysis time were considered, so that just four OMI orbits worth of data per day were used (or about 30% of the available OMI data). No time interpolation was performed given the short time interval between each satellite measurement and analysis time (less than 1 h)

Figure 1. OMI ozone total column averaging kernels or layer efficiency factors, defined on 11 atmospheric layers, for OMI observation at the nadir position on 15 October 2005 between 1135 and 1230 UTC. Above each figure is indicated the lower and upper pressure level values delimiting each layer (in hPa). At high latitude, here corresponding to high solar zenith angle, the averaging kernels for the lower layers are smaller than one, i.e., measurements are less sensitive to ozone partial column variations. This is likely to be due to Rayleigh scattering and clouds. In particular, the averaging kernel for the lowest layer is smaller at most latitudes. In higher layers, however, starting from the middle stratosphere, the averaging kernels at high solar zenith angle are greater than one: a low ozone partial column a priori estimate gives rise to an overestimation of the total ozone column [*Bhartia and Wellemeyer*, 2002].

with respect to the 6-h analysis time interval. For each OMI ozone column in the intercomparison data set, profiles of ozone mixing ratios from the model analysis were horizontally interpolated onto OMI pixel locations. Mixing ratio profiles were then converted to ozone partial columns, denoted as $\mathbf{x}_{\text{ana}}$, by integrating them over the 11 vertical layers where OMI a priori and total column averaging kernel profiles are defined.

[21] Similarly to a satellite retrieval, the analysis is an estimate of a field given by constraining the available observations with some prior information, here in the form of a short-range forecast and its error covariance matrix. This means that the analysis is only an indirect estimate of the state of the atmosphere with finite spatial resolution as determined by a set of averaging kernel functions. In principle then, the problem of intercomparing model analyses to remote sensing measurements should be addressed in the same way as the one of intercomparing two remote sounders. But while the true state for a given atmospheric parameter represents an atmospheric profile along the instrument line of sight in the case of remote sounding data, it represents the whole atmosphere in the case of a numerical weather prediction analysis. The size of the analysis averaging kernel matrix is too large to allow the matrix elements to be computed.

[22] A simplified approach is adopted whereby the analysis averaging kernel matrix is assumed to be block diagonal reflecting a unit matrix in the vertical and no correlation between different horizontal locations. Ozone analyses were then treated as if they represented direct estimates of ozone partial columns independent of neighboring ozone column estimates:

$$\mathbf{x}_{\text{ana}} = \mathbf{x} + \boldsymbol{\epsilon}_{\text{ana}} \tag{3}$$

where $\boldsymbol{\epsilon}_{\text{ana}}$ is a profile of the analysis error at the considered location. Let us now define $\hat{\Omega}_{\text{ana}}$, the simulated OMI column, as

$$\hat{\Omega}_{\text{ana}} = \Omega_a + \mathbf{a}^T(\mathbf{x}_{\text{ana}} - \mathbf{x}_a) \tag{4}$$

where $\mathbf{a}$ and Ω_a are the total column averaging kernel and the a priori total column, respectively, valid for the OMI pixel at the considered location. If equation (3) is inserted into equation (2) [e.g., *Migliorini et al.*, 2004], the difference $\delta\hat{\Omega}$ between co-located actual and simulated OMTO3 measurements can be written as

$$\delta\hat{\Omega} \equiv \hat{\Omega}_{\text{OMI}} - \hat{\Omega}_{\text{ana}} = -\mathbf{a}^T\boldsymbol{\epsilon}_{\text{ana}} + \epsilon_\Omega + \epsilon_R \tag{5}$$

where ϵ_R is the representativeness error [e.g., *Cohn*, 1997], an error due to the limited resolution of the model analyses which cannot capture the subgrid-scale variability of ozone columns revealed by the observations. The resolution of the spectral model (T159) used in this work corresponds to about 125 km × 125 km at the equator [e.g., *Laprise*, 1992]. This means that, at the equator, OMTO3 pixels at nadir are about 50 times smaller than the analysis grid resolution. Representativeness error is then likely to be an important source of error that needs to be taken into account, as discussed in section 3.1.

[23] Let us define $\mu = E\{\delta\hat{\Omega}\}$ and $\sigma^2 = E\{(\delta\hat{\Omega} - \mu)^2\}$ as the expectation and the variance of $\delta\hat{\Omega}$, respectively. From equation (5), it follows that

$$\mu = -\mathbf{a}^T\boldsymbol{\mu}_{\text{ana}} + \mu_\Omega + \mu_R \tag{6}$$

where $\boldsymbol{\mu}_{\text{ana}} = E\{\epsilon_{\text{ana}}\}$ is the analysis bias vector, $\mu_\Omega = E\{\epsilon_\Omega\}$ is the OMI ozone total column bias, and $\mu_R = E\{\epsilon_R\}$ is the representativeness error bias. Assuming all errors are mutually uncorrelated, it follows that

$$\sigma^2 = \mathbf{a}^T\mathbf{S}_{\text{ana}}\mathbf{a} + \sigma_\Omega^2 + \sigma_R^2 \tag{7}$$

where $\mathbf{S}_{\text{ana}}$ is the vertical analysis error covariance, $\sigma_\Omega^2 = E\{(\epsilon_\Omega - \mu_\Omega)^2\}$ the OMI total column error variance and $\sigma_R^2 = E\{(\epsilon_R - \mu_R)^2\}$ the representativeness error variance. From our definitions, it follows that the root-mean-square error (RMSE), square root of the quadratic mean $E\{\delta\hat{\Omega}_2\}$, can be written as RMSE = $\sqrt{\sigma^2 + \mu^2}$. It is also useful to define the analogous relative quantities: the relative bias $\mu_{\text{rel}} = E\{\delta\hat{\Omega}/\hat{\Omega}_{\text{ana}}\}$, the relative variance $\sigma_{\text{rel}}^2 = E\{(\delta\hat{\Omega}/\hat{\Omega}_{\text{ana}} - \mu_{\text{rel}})^2\}$, and the relative root-mean-square error $\text{RMSE}_{\text{rel}} = \sqrt{\sigma_{\text{rel}}^2 + \mu_{\text{rel}}^2}$. Finally, the correlation coefficient r between measured and simulated OMI ozone total columns can be written in our notation as

$$r = \frac{E\{\left(\hat{\Omega}_{\text{OMI}} - E\{\hat{\Omega}_{\text{OMI}}\}\right)\left(\hat{\Omega}_{\text{ana}} - E\{\hat{\Omega}_{\text{ana}}\}\right)\}}{\sqrt{E\{\left(\hat{\Omega}_{\text{OMI}} - E\{\hat{\Omega}_{\text{OMI}}\}\right)^2\}E\{\left(\hat{\Omega}_{\text{ana}} - E\{\hat{\Omega}_{\text{ana}}\}\right)^2\}}} \tag{8}$$

[24] Absolute and relative bias and RMSE values as well as correlation coefficients are estimated for each OMI orbit within the whole comparison data set by means of the sample mean $\hat{\mu}$, the sample variance $\hat{\sigma}^2$ and the sample covariance, each with their own precision. From these quantities, it is then possible to evaluate the time dependence of the distribution of total column (relative) differences. For example, we may want to check whether the first two moments of the distribution are constant in time, thereby describing a stationary process, or vary slowly over a given period. In these cases, it may be useful to calculate specific parameters of the distribution of the differences relative to the selected period. Note in particular that the bias $\langle\mu\rangle$ and root-mean-square error $\langle\text{RMSE}\rangle$ averaged over M orbits can be calculated from the bias $\hat{\mu}$ and root-mean-square error $\hat{\text{RMSE}}$ already computed for each orbit as

$$\langle\mu\rangle = \frac{\sum_{k=1}^{M} N_k\hat{\mu}_k}{\sum_{k=1}^{M} N_k} \tag{9}$$

$$\langle\text{RMSE}\rangle = \sqrt{\frac{\sum_{k=1}^{M} N_k\hat{\text{RMSE}}_k^2}{\sum_{k=1}^{M} N_k}} \tag{10}$$

where N_k is the number of column differences for the kth OMI orbit. A similar statistical analysis was carried out for OMI and analysis columns within a set of five latitude bands encompassing the whole globe to check for a possible latitudinal dependence of the intercomparison results.

Table 1. Geographical Locations of the Brewer Instruments Available at Aura Validation Data Center for the Period Between 12 August 2005 and 31 October 2005[a]

Location	Longitude (deg)	Latitude (deg)	N
Toronto	−79.468	43.781	124
Saturna Island	−123.128	48.775	127
Goose Bay	−60.300	53.317	130
Churchill	−94.074	58.739	37
Edmonton	−114.109	53.548	86
Eureka	−85.940	79.988	7
Regina	−104.713	50.204	141

[a]For each instrument, *N* measurements satisfying our colocation criterion were considered (see text).

[25] As anticipated in section 1, the analysis error covariance matrix is not provided by the DAS used in this work. This means, for example, that it is not possible to check whether each difference $\delta\hat{\Omega}$ is normally distributed with variance σ^2 given by equation (7) even when the resolution of the analysis grid is high enough to make representativeness errors negligible. However, an estimate of σ^2 can provide an upper limit estimate of the variance of the OMI total column error variance σ^2_Ω.

3.1. Evaluation of the Systematic Error Component

[26] In general, both measurement and analysis errors may have a systematic component, e.g., due to errors in parameters used to calibrate satellite observations that are used for assimilation. Let us consider an ensemble of n column differences $\delta\hat{\Omega}$, as taken say from the N_k differences in the kth OMI orbit of the data set. From equation (5), the ensemble mean, denoted by an overbar, of the n column differences $\delta\hat{\Omega}$ can be written as

$$\overline{\delta\hat{\Omega}} = \overline{\epsilon_{\mathrm{rnd}}} + \overline{\epsilon_{\mathrm{sys}}} \tag{11}$$

where ϵ_{rnd} and ϵ_{sys} are the random and the systematic error components of the column difference $\delta\hat{\Omega}$, respectively. The random error has a known variance $\sigma^2(\epsilon_{\mathrm{rnd}})$, while systematic errors are assumed constant and treated as they had a (known) variance $\sigma^2(\epsilon_{\mathrm{sys}})$.

[27] An important property of the ensemble mean of random errors is that its probability distribution function has a variance that scales with the number of ensemble members. On the other hand, in the case of systematic errors the variance of the mean remains unchanged regardless the size of the ensemble [e.g., *Taylor*, 1997, section 4.6]. This means that $\sigma^2\left(\overline{\delta\hat{\Omega}}\right)$, the variance of the mean of the ensemble of n column differences $\delta\hat{\Omega}$ can be written as

$$\sigma^2\left(\overline{\delta\hat{\Omega}}\right) = \frac{\sigma^2(\epsilon_{\mathrm{rnd}})}{n} + \sigma^2(\epsilon_{\mathrm{sys}}) \tag{12}$$

The variance of ϵ_{sys} can then be estimated as the lower limit of $\sigma^2\left(\overline{\delta\hat{\Omega}}\right)$ for an increasing number of ensemble members, belonging, for example, to the same OMI orbit, used to calculate $\overline{\delta\hat{\Omega}}$. The total error on the sample mean $\hat{\mu} \equiv \overline{\delta\hat{\Omega}}$ can be calculated as

$$\Delta\mu = \sqrt{\frac{\sigma^2(\epsilon_{\mathrm{rnd}})}{N} + \sigma^2(\epsilon_{\mathrm{sys}})} \tag{13}$$

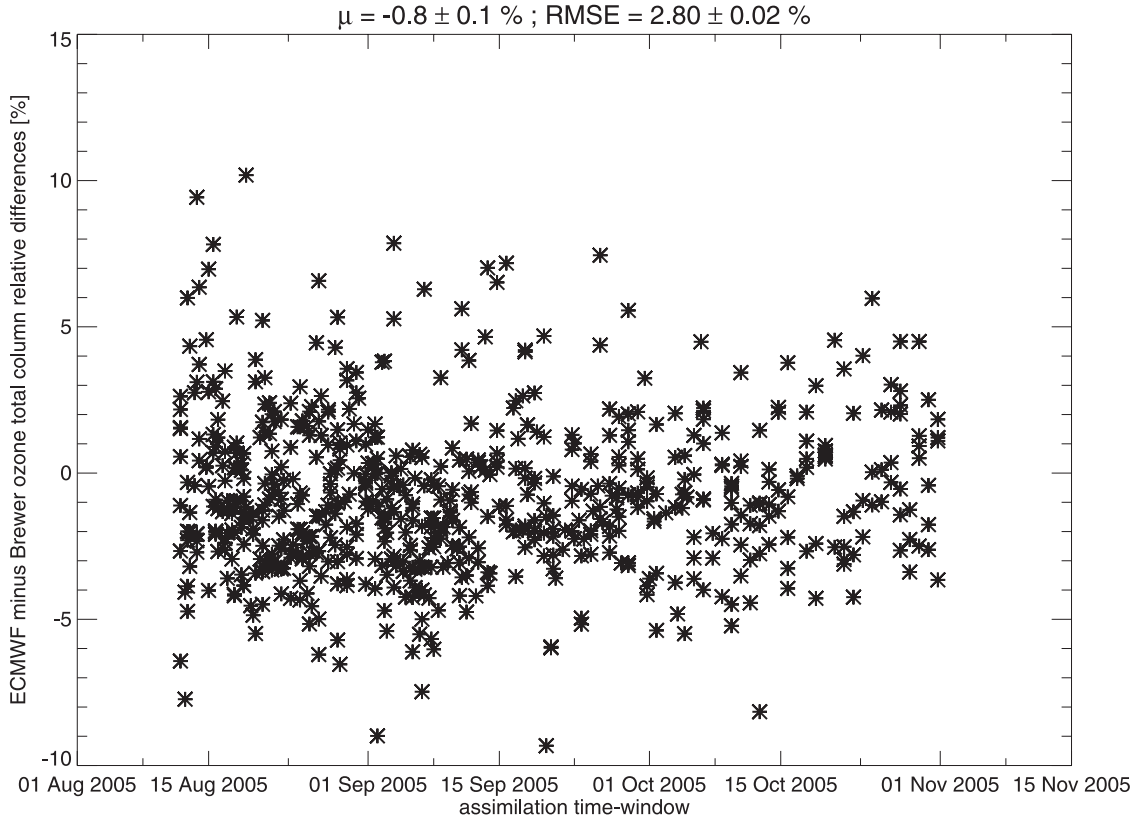

Figure 2. Time series of relative differences between ECMWF and Brewer ozone total columns for a total of 652 coincidences between 12 August and 31 October 2005.

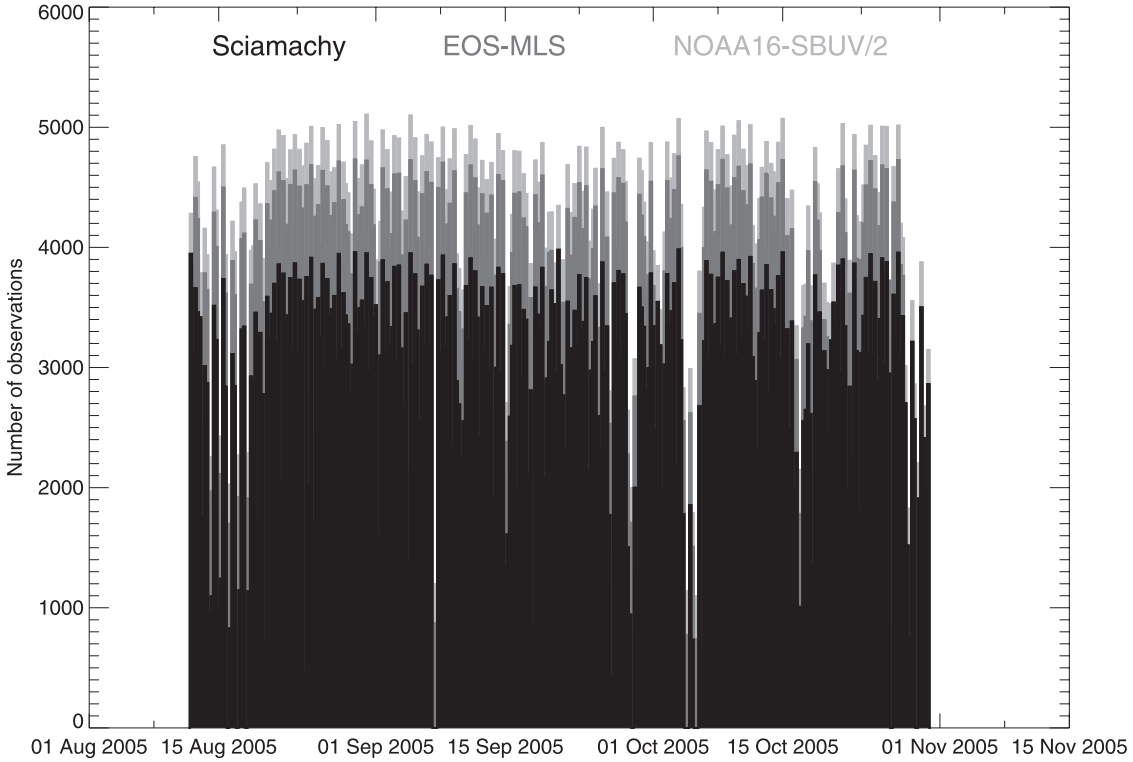

Figure 3. Time series of the total number of ozone sensitive observations available for assimilation in each 6-h assimilation window between 12 August and 31 October 2005. Each bar is colored according to the number of observations available from SCIAMACHY (black), EOS/MLS (dark grey), and SBUV/2 (grey).

where N is the number of column difference used to estimate $\hat{\mu}$. An expression for the total error on the sample root-mean-square error $\hat{\text{RMSE}} \equiv \left(\overline{\delta\hat{\Omega}^2}\right)^{1/2}$ is derived in Appendix A.

[28] In equation (5), a representativeness error term ϵ_R was introduced. When the atmospheric field can be regarded as homogeneous, ϵ_R can be considered as a random variable with zero mean and given (e.g., climatological) error variance [*Cohn*, 1997, section 6.3]. However, in general, ϵ_R will have a state dependent mean [*Cohn*, 1997, section 6.4] that is constant for a given mean small-scale atmospheric field. This means that in general, ϵ_R should be considered as a systematic error. In our particular example ϵ_R is likely to be systematically larger over regions of high ozone and temperature variability (e.g., around filaments or at the edge of the stratospheric vortex) and smaller where fields experience larger-scale variations (as in the case of ozone in the tropics). An estimate of the variance of ϵ_{sys} is then an estimate of the sum of the representativeness error variance and of the variance of all other sources of systematic errors in the ozone columns comparison ensemble. The determination of the systematic error standard deviation is presented as part of section 4.3. Earlier error estimations refer only to the random error component.

4. Results

[29] Our data set consisted of 210 colocated OMI orbits and ozone analyses. Ozone observations used for assimilation and short-range model forecasts at observation locations and times were also available. A subset of the analysis data set was used to quantify the level of agreement between actual and simulated OMI ozone total columns. However, before analyzing the results of the comparison between analyses and OMI data, it is first necessary to assess the quality of the ozone analyses and also to verify the consistency between the assimilated ozone data set and the ozone predictions made using the ECMWF model.

4.1. Evaluation of the Analysis Data Set

[30] In section 2.1, results of a comparison between ECMWF ozone columns in ERA-40 and independent observations are summarized. Here we discuss a similar intercomparison that is valid for the case study investigated in this paper. Ozone total columns from Brewer spectrophotometers for the period 12 August 2005 to 31 October 2005 obtained from the Aura Validation Data Center (AVDC) were chosen as our independent set of ozone observations, given that they are not routinely assimilated at ECMWF. Only data within an hour from each analysis time and characterized by a solar zenith angles not greater than 70° was considered for a total of 652 comparisons. The weighted least squares estimate was considered when, for a specific comparison, more than one Brewer measurement was within our selection criterion. In Table 1, the locations of the instruments and the number of measurements (or least squares estimates) used for evaluating our ECMWF analysis data set are shown. Note that at the time of our investigation, only stations in Canada were available from AVDC for

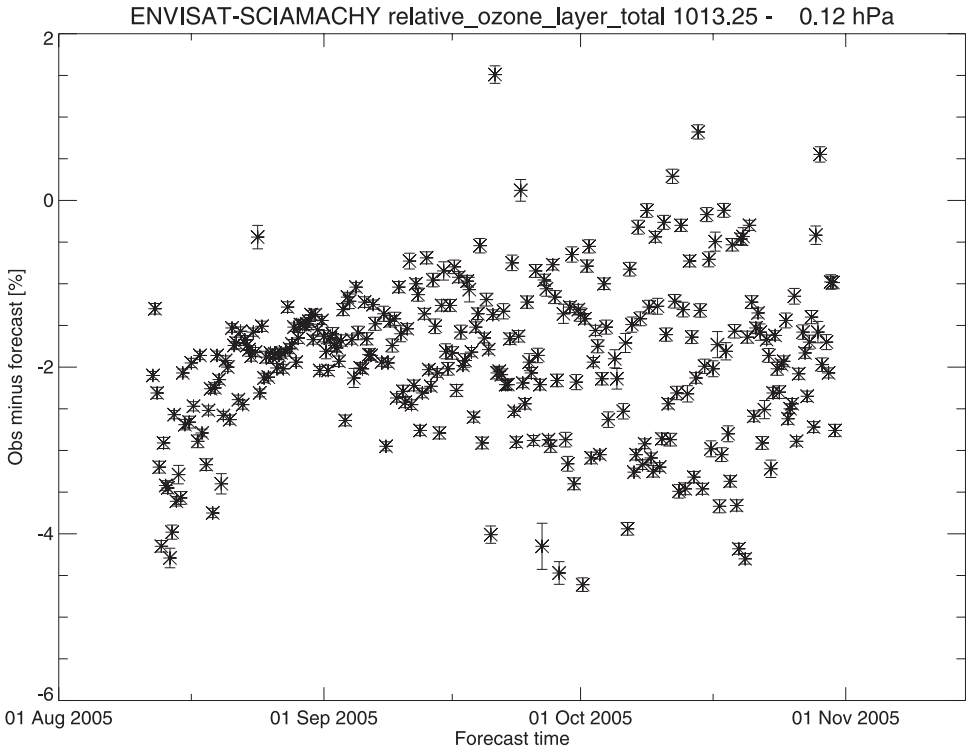

Figure 4. Time series of the relative innovations in each 6-h assimilation window between 12 August and 31 October 2005 for SCIAMACHY data retrieved with the "Total Ozone retrieval scheme for SCIAMACHY based on the OMI DOAS algorithm" (TOSOMI).

our case study period. Although the geographical extension of the area where the global ozone analyses were evaluated is rather limited, the total number of considered Brewer measurements is large enough to make our comparison statistically significant.

[31] In Figure 2, the differences between ECMWF ozone total columns interpolated at Brewer instruments locations and the ozone total columns from Brewer instruments within the coincidence criterion, divided by the ozone total columns from Brewer instruments, or relative differences between ECMWF and Brewer ozone total columns, are shown as a function of the analysis time. The statistical distribution of the comparison is characterized by a bias $\langle\mu\rangle = -0.8 \pm 0.1\%$ and a $\langle\text{RMSE}\rangle = 2.80 \pm 0.03\%$.

[32] The 1σ error for direct sun observations made with a well-calibrated Brewer instrument is estimated to be about 1% for daily mean values and is slightly higher (about 1.5%) for individual measurements [*Fioletov et al.*, 2005]. This means that it is possible to make use of ECMWF ozone analyses to highlight possible OMI ozone column biases. However, the RMSE resulting from our intercomparison is larger than 2%, the minimum accuracy required from OMI to extend the TOMS ozone record [*Levelt et al.*, 2006b]. Therefore, the estimated accuracy of ECMWF ozone analyses is not adequate for using ECMWF ozone total columns to confirm whether such a goal can be reached.

4.2. Evaluation of the Innovations

[33] Let us now investigate the statistical properties of the innovation sequences for our ozone assimilation data set including SCIAMACHY ozone total columns and EOS-MLS and SBUV/2 ozone partial columns. Figure 3 shows the number of available observations for the three instruments. It is evident that SCIAMACHY is the main provider of ozone observations, albeit with very limited vertical resolution.

[34] In Figure 4, the relative innovations d or relative differences between SCIAMACHY ozone column estimates $\hat{\Omega}$ and ECMWF ozone column forecasts at observation times and locations Ω_f, defined as $d = (\hat{\Omega} - \Omega_f)/\Omega_f$, are shown as percentages. Note that over the initial part of the assimilation experiment, the innovations seem to show an increasing trend: this "spin-up" period is a typical signature of assimilation of new observations into a model when initial conditions for predictions at the beginning of the experiment are generated without those measurements. In the present assimilation run, the initial conditions are represented by an operational ECMWF analysis generated without EOS MLS measurements. Newly assimilated observations have initially larger differences in magnitude from the ozone values predicted by the model. As the assimilation progresses, the ozone analyses, on average, get closer to the values predicted by the observations, even though the spread seems to increase. Note that at the time when the assimilation runs were performed, MLS ozone retrievals from 28 October 2005 to the end of the run were not yet available and so were not assimilated during that period.

[35] On the basis of these considerations, confirmed by the results shown in Figure 5 and discussed in section 4.3, time-averaged statistical figures were calculated for this paper only from data that refer to the period between 23 September and 27 October 2005 in order to avoid the spin-

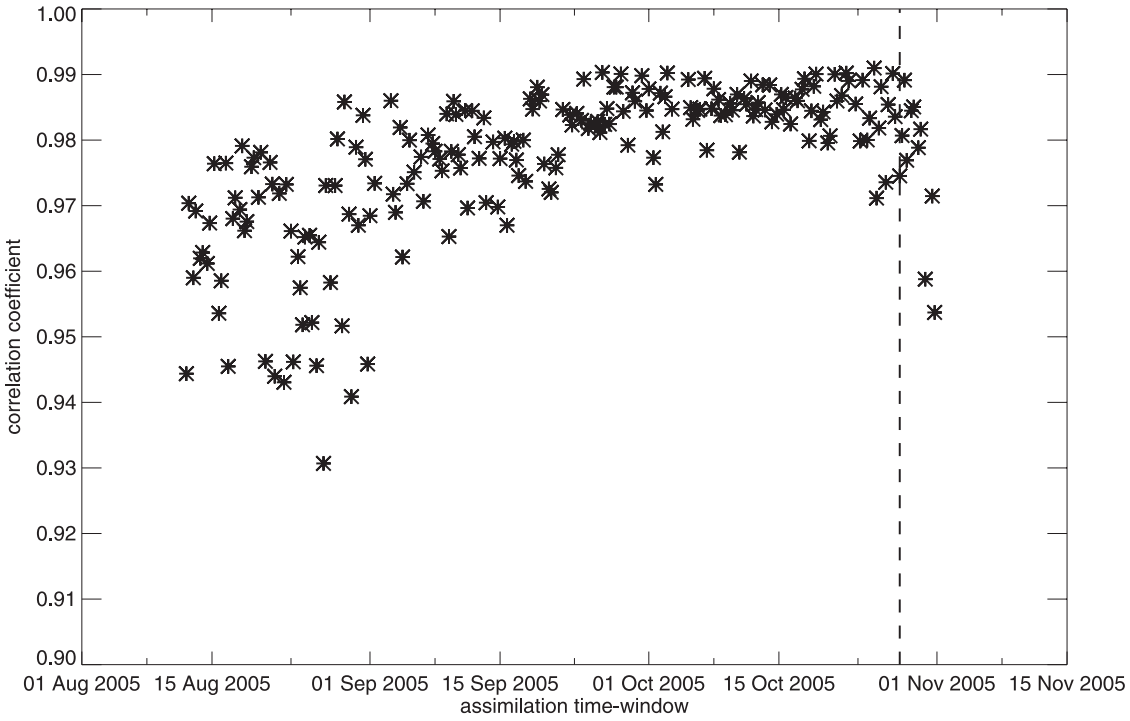

Figure 5. Time series of the correlation coefficient between actual and simulated OMI OMTO3 columns. There are a total of 210 coincidences between 12 August and 31 October 2005. The vertical dashed line indicates when MLS ozone retrievals have stopped being assimilated (28 October): the subsequent correlation values decrease sharply.

up period and the loss of MLS data. The time-averaged SCIAMACHY relative innovation value $\langle \mu_d \rangle$ calculated from equation (9) is equal to $\langle \mu_d \rangle = -1.897 \pm 0.004\%$; innovations are found to be more negatively biased over the tropics when time averages are instead calculated over latitude bands. It follows that when SCIAMACHY observations are assimilated, they are likely to produce an analysis with ozone total column values that are lower than those that would be forecast by the model on its own and particularly so in the tropics.

[36] In order to have a better understanding of our findings, let us discuss the case when just a single SCIAMACHY ozone column $\hat{\Omega}$ is assimilated. For simplicity, it is also assumed that the estimate can be expressed as $\hat{\Omega} = \Omega + \epsilon_\Omega$ (see equation (2) and subsequent discussion). In this case, the total column ozone analysis $\hat{\Omega}_{\text{ana}}$ at observation location can be expressed as [e.g., *Daley*, 1991, section 4.6] $\hat{\Omega}_{\text{ana}} = \Omega_f + k(\hat{\Omega} - \Omega_f)$, with $k = \sigma_f^2/(\sigma_\Omega^2 + \sigma_f^2)$ and $0 < k < 1$. Here, Ω_f is the total column ozone forecast at the observation location, while σ_f^2 and σ_Ω^2 are the total column ozone forecast error variance and the total column ozone observation error variance, respectively. It follows that $\epsilon_{\Omega_{\text{ana}}} = k\epsilon_\Omega + (1 - k)\,\epsilon_{\Omega_f}$, where $\epsilon_{\Omega_{\text{ana}}}$ and ϵ_{Ω_f} are the total column ozone analysis and forecast errors, respectively. When expectations are calculated, we get $\mu_{\Omega_{\text{ana}}} = k\mu_\Omega + (1 - k)\mu_{\Omega_f}$ where μ denotes a bias. The innovation bias μ_d is defined as $\mu_d = E\{\hat{\Omega} - \Omega_f\} = \mu_\Omega - \mu_{\Omega_f}$. Let us now assume that there is no forecast bias, i.e., $\mu_{\Omega_f} = 0$, so that $\mu_d = \mu_\Omega$ and $\mu_{\Omega_{\text{ana}}} = k\mu_\Omega$. From $k < 1$ it follows that $|\mu_{\Omega_{\text{ana}}}| < |\mu_d| = |\mu_\Omega|$. Now, as discussed in section 4.1, the analysis has a negative bias with respect to Brewer observations, albeit determined over a limited geographical area, and this bias is smaller in magnitude than the mean SCIAMACHY innovation. This means that our results could be explained by assuming that the bias between the analyses and the Brewer observations is due to a (larger in magnitude) SCIAMACHY negative bias, of the order of our estimated SCIAMACHY innovation bias. A good way to support such a conclusion is to

Table 2. Estimates of the Relative Bias $\langle \mu_d \rangle$ and of the Relative Root-Mean-Square Error $\langle \text{RMSE}_d \rangle$ of N MLS Innovations Averaged Over the Period Between 23 September and 27 October 2005[a]

δp (hPa)	$\langle \mu_d \rangle$ (%)	$\langle \text{RMSE}_d \rangle$ (%)	$\langle \Delta\hat{\Omega} \rangle$ (DU)	N (10^4)
0.46–0.68	−2.56 ± 0.04	11.05	0.35 ± 0.05	6.52
0.68–1.00	−9.04 ± 0.04	13.19	0.64 ± 0.07	6.54
1.00–1.46	−17.05 ± 0.03	19.10	1.21 ± 0.10	6.55
1.46–2.15	−15.26 ± 0.03	17.11	2.37 ± 0.13	6.55
2.15–3.16	−12.26 ± 0.02	13.83	4.49 ± 0.18	6.55
3.16–4.64	−7.99 ± 0.02	9.97	7.78 ± 0.26	6.55
4.64–6.81	−7.30 ± 0.02	9.50	12.26 ± 0.37	6.55
6.81–10.00	−2.95 ± 0.03	7.09	18.07 ± 0.52	6.55
10.00–14.67	**−0.13** ± 0.02	5.92	25.13 ± 0.65	6.55
14.67–21.54	**0.90** ± 0.02	5.38	31.59 ± 0.71	6.55
21.54–31.62	**0.40** ± 0.03	7.06	34.60 ± 0.72	6.51
31.62–46.41	**1.62** ± 0.06	14.26	34.40 ± 0.75	6.43
46.41–68.12	**0.18** ± 0.06	15.71	30.71 ± 0.78	6.36
68.12–100.00	**0.32** ± 0.07	15.58	22.32 ± 0.84	5.58
100.00–146.78	5.76 ± 0.14	34.06	15.25 ± 0.93	5.50
146.78–215.44	25.57 ± 0.59	138.70	12.62 ± 1.24	5.36

[a]Results are shown for a given atmospheric layer defined by the pressure interval δp characterized by an average ozone partial column $\langle \Delta\hat{\Omega} \rangle$. Relative bias values for layer-averaged ozone partial column greater than 20 DU are shown in bold. Note that provided RMSE estimates are accurate to better than two significant digits, when only random errors are considered.

Table 3. Estimates of the Relative Bias $\langle \mu_d \rangle$ and of the Relative Root-Mean-Square Error $\langle \mathrm{RMSE}_d \rangle$ of N SBUV/2 Innovations Averaged Over the Period Between 23 September and 27 October 2005[a]

δp (hPa)	$\langle \mu_d \rangle$ (%)	$\langle \mathrm{RMSE}_d \rangle$ (%)	$\langle \Delta\hat{\Omega} \rangle$ (DU)	N (10^4)
0.12–0.99	6.02 ± 0.04	9.19	1.47 ± 0.11	2.82
0.99–1.98	6.13 ± 0.04	9.07	3.76 ± 0.19	2.82
1.98–3.96	3.09 ± 0.03	6.63	10.92 ± 0.44	2.82
3.96–7.92	**3.55** ± 0.03	6.01	25.08 ± 1.21	2.82
7.92–15.83	**7.35** ± 0.03	9.14	46.86 ± 3.23	2.82
15.83–1013.25	**2.05** ± 0.03	5.81	205.18 ± 30.80	2.82

[a]Results are shown for a given atmospheric layer defined by the pressure interval δp and characterized by an average estimated ozone partial column given by $\langle \Delta\hat{\Omega} \rangle$. Relative bias values for layer-averaged ozone partial column greater than 20 DU are shown in bold. Note that provided RMSE estimates are accurate to better than two significant digits, when only random errors are considered.

compare SCIAMACHY total columns retrieved with the same algorithm to independent data. *Eskes et al.* [2005] compared TOSOMI data taken during 2003 and 2004 with ground-based measurements at seventy ground locations from Dobson, Brewer, and Filter instruments. They found that SCIAMACHY data have a bias of −1.7%, which is remarkably close to our estimated mean SCIAMACHY innovation.

[37] So far, no mention has been made of the possible role of MLS and SBUV/2 observations in the analysis bias. In Tables 2 and 3, the time-averaged relative innovations for ozone partial columns from MLS and SBUV/2 are shown. A 0.55 ± 0.02% mean relative innovation is found when a weighted average of the MLS mean relative innovations is calculated for layer-averaged measured partial ozone columns $\langle \delta\hat{\Omega} \rangle$ greater than 20 DU. When a similar figure is calculated for SBUV/2 innovations, we get a mean value of 4.32 ± 0.02%.

[38] These results show that, on average, MLS ozone measurements agree reasonably well with the model ozone forecasts. This is likely to arise from these two facts: MLS measures ozone partial columns with errors (shown in Table 2) that, in the region of the atmosphere where the partial column values are largest, are significantly less than about 6%, the average SCIAMACHY ozone total column relative error for the SCIAMACHY observations within our assimilation data set; MLS provides good vertical resolution as compared to resolutions from nadir sounders such as SCIAMACHY and SBUV/2. Conversely, SBUV/2 ozone measurements are, on average, significantly greater than the model ozone forecasts. This is reasonable since SBUV/2 partial ozone column errors (shown in Table 3) are either comparable or, below 15.83 hPa, where most of the ozone is concentrated, significantly larger than average SCIAMACHY errors. This means that the relatively small number of SBUV/2 observations available in our data sets is neither compensated by their precision nor their vertical resolution as it is in the case of MLS observations.

4.3. Evaluation of OMI Ozone Data

[39] Figure 5 provides the linear correlation coefficient as a function of time describing the correlation between observed and simulated OMI ozone columns. For each OMI orbit, the average number of comparisons or ozone column differences is about 82,000 with a standard

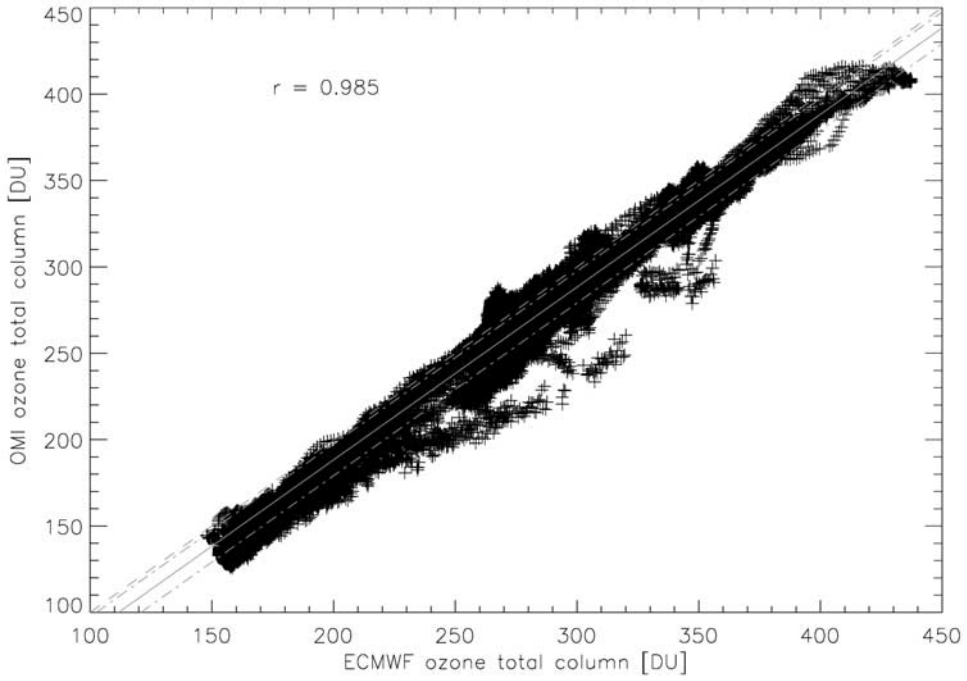

Figure 6. Scatterplot of measured and simulated OMTO3 ozone column data during the coincidence on 15 October 2005 around 1200 UTC. The dashed line marks where the values are the same; the solid line marks the mean difference between measured and simulated OMTO3 ozone columns; the dashed-dotted lines determine the 1-σ confidence area. The correlation coefficient r has a value of 0.985.

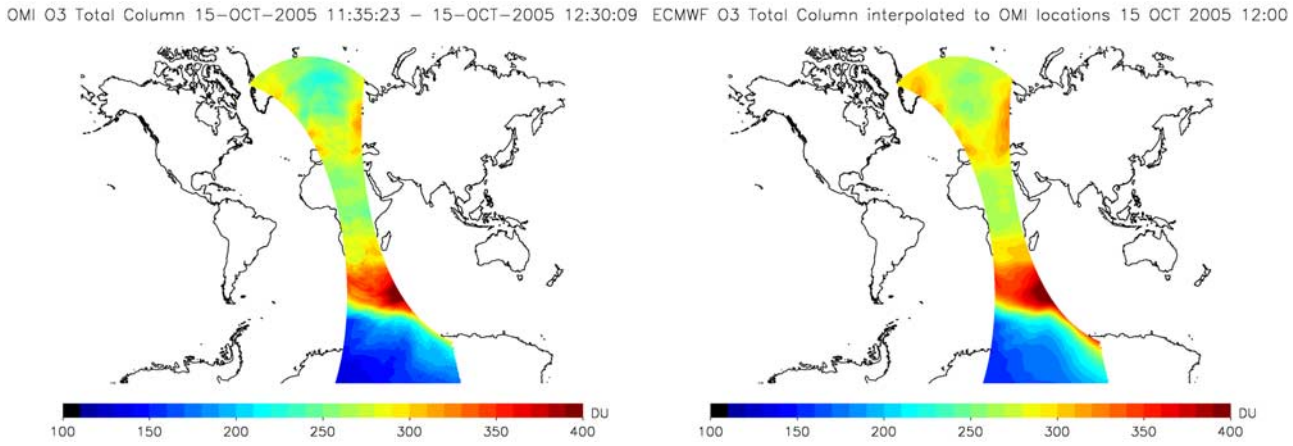

Figure 7. (left) OMI ozone total columns (OMTO3) for the orbit on 15 October 2005 between 1135 and 1230 UTC; (right) OMI total columns simulated according to equation (4) by means of the ECMWF ozone analysis valid at 1200 UTC on 15 October 2005.

deviation of about 1000: the population of the ensemble of differences is fairly constant over the assimilation experiment.

[40] The figure shows that even though the correlation r is always very high ($r > 0.93$), there is a very evident correlation gain during the first 40 days of assimilation, i.e., the spin-up period defined in section 4.2. From 28 October 2005 (a date marked in Figure 5 with a vertical dashed line) to the end of the experiment, a loss of correlation is experienced and this provides an indication for MLS ozone data being highly correlated with OMI ozone columns and of the importance of MLS data for constraining the ozone analyses.

[41] It is useful to perform a more detailed analysis of the column differences on a given assimilation window. Here, we arbitrarily selected the window centered on 15 October 2005 1200 UTC within the period when the correlation is at its saturation level. In Figure 6, a scatterplot of OMI versus simulated OMI ozone columns is shown. In this case, $r = 0.985$ and the values appear to be more correlated for both low and high column amounts.

[42] Figure 7 shows the OMI ozone columns measured on 15 October 2005 between 1135 and 1230 UTC (Figure 7, left) and the simulated OMI columns at 1200 UTC on the same day, interpolated to the OMI observation locations (Figure 7, right). It can be seen that the highly correlated high and low column values are mainly concentrated in the southern hemisphere. In this region, it is possible to highlight at least three features. These are listed below.

[43] 1. The position of the edge of the SH polar vortex as measured by OMI agrees very well with that prescribed by the analysis.

[44] 2. The OMI spatial distribution of high ozone column values north of the vortex edge closely follows the analysis despite the fact that the resolution of the model is significantly lower than that of OMI.

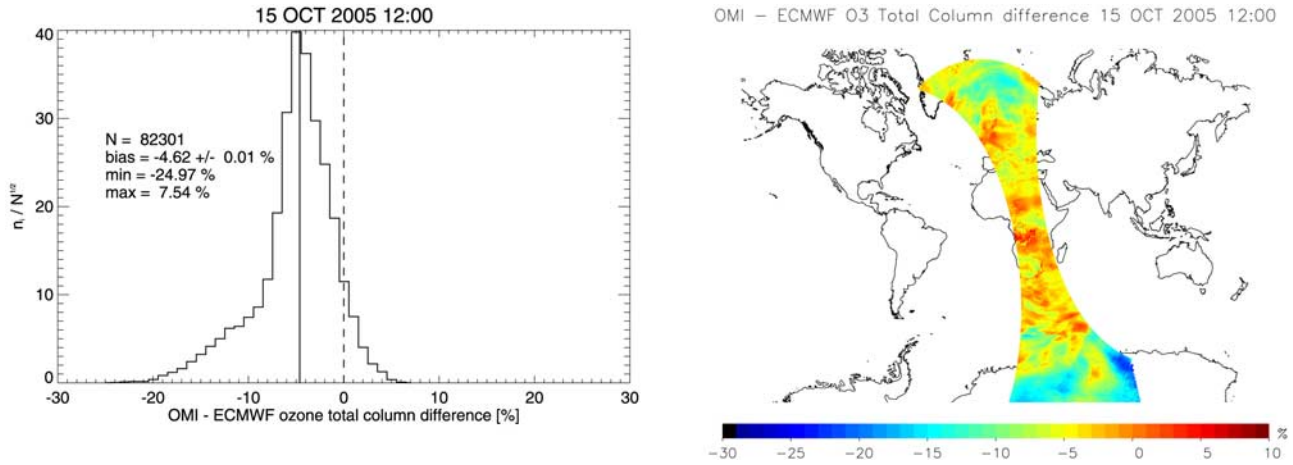

Figure 8. (left) Histogram and (right) geographical distribution of measured minus simulated OMI ozone total column relative differences for the coincidence on 15 October 2005 around 1200 UTC. The total number N of column differences is $N = 82301$ and it results in a negative bias $\mu = -4.62 \pm 0.01\%$ (marked by the vertical solid line), where the quoted error represents the random component of the total error only. Relative differences are always greater than -25% and smaller than 8%. Difference values that are largest in magnitude are mainly located at high latitudes.

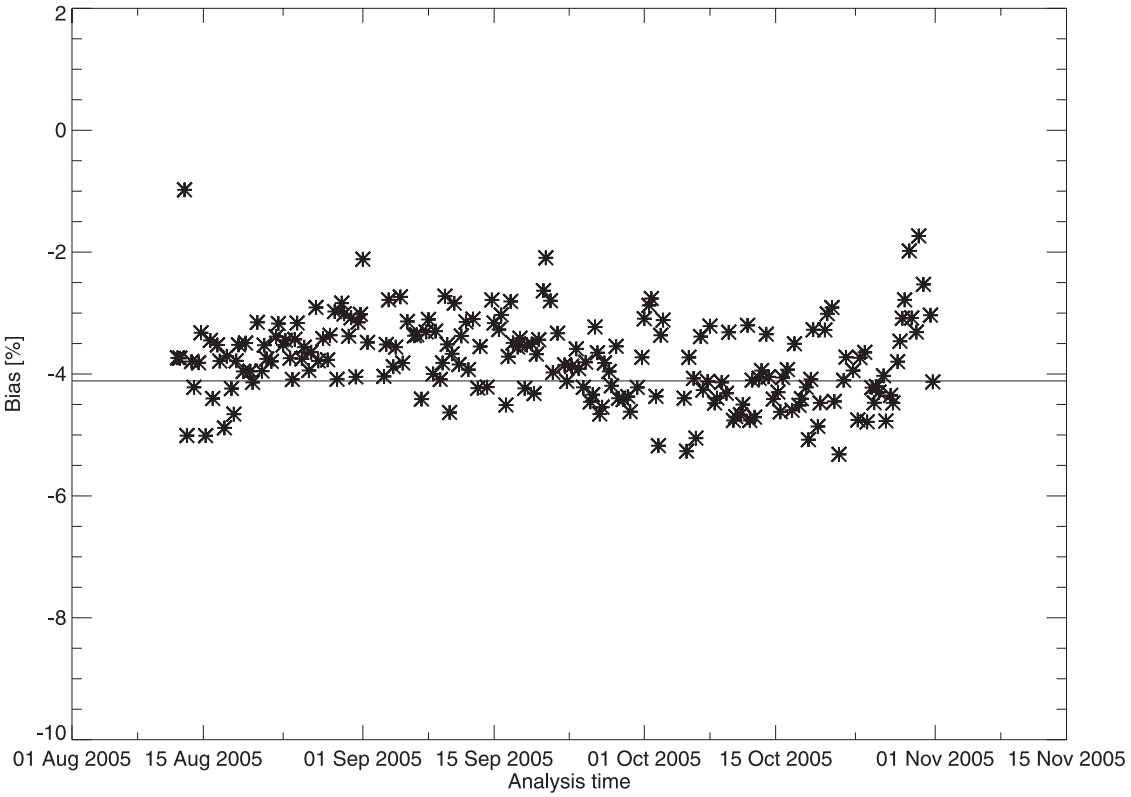

Figure 9. Time series of the relative bias $\mu_{\mathrm{rel}} = E\{\delta\hat{\Omega}/\hat{\Omega}_{ana}\}$ (in %) between actual and simulated OMI OMTO3 data. A total of 210 coincidences between 12 August and 31 October 2005 is shown. The solid horizontal line marks the value of the relative bias $\langle\mu_{\mathrm{rel}}\rangle = -4.11\%$.

[45] 3. The ozone gradient from the edge towards the center of the vortex as measured by OMI appears to be steeper than the one inferred from the analysis, indicating that OMI provides a lower estimate of the amount of ozone inside the vortex.

[46] In order to provide a more quantitative insight, Figure 8 (left) presents a histogram of the actual distribution of relative column differences. The relative differences of the columns never differ by more than 25% in magnitude, with more than half of the total OMI values being smaller than the corresponding analysis ozone field, and this is reflected by the presence of a significant negative bias ($\mu = -4.62 \pm 0.01\%$). The RMSE is found to be equal to 6.18%. From Figure 8 (right), there is also an indication that most of the largest relative discrepancies are located at high latitudes. In particular, the outliers of the distribution of relative differences, here defined as relative differences exceeding a 4σ threshold, where σ is the standard deviation of the distribution, happen to be located in a region that is both close to the southern hemisphere vortex and where the solar zenith angles (SZA) at the satellite instrument are high (SZA $> 78^\circ$ for most outliers) as seen in the bottom-right corner of Figure 7 (left and right) and Figure 8 (right).

[47] The statistical results presented above only refer to a single OMI orbit. A statistical analysis over the whole assimilation period when taking into account all sources of errors is needed to get a robust estimate of the accuracy of the measured OMI columns with respect to the simulated OMI columns. In Figures 9 and 10, time series of relative bias and RMSE values are shown. Here, the initial spin-up period is of the order of ten days, much shorter than for the correlation coefficient time series. This may be due to the short time scale variability of the bias and RMSE (of the order of a few 6-hourly assimilation time windows) being larger than the reduction in RMSE and in the magnitude of the bias resulting from the assimilation of MLS ozone measurements during the initial spin-up phase. After this initial period, the bias and RMSE do not show significant temporal variations. The mean bias and RMSE, calculated from equations (9) and (10), and denoted by a solid horizontal line in the plots of the relative bias and RMSE, are: $\langle\mu\rangle = -11.387 \pm 0.004$ DU or $\langle\mu_{\mathrm{rel}}\rangle = -4.113 \pm 0.004\%$ and $\langle\mathrm{RMSE}\rangle = 15.2$ DU or $\langle\mathrm{RMSE}_{\mathrm{rel}}\rangle = 5.6\%$.

[48] So far, only the random error component of the mean bias was considered, being easily determined from the distribution of the column differences. But, as discussed in section 3.1, this error may seriously underestimate the accuracy of the comparison. The systematic component of the total error was estimated as follows. For each OMI orbit in the comparison data set, the distribution of $\delta\hat{\Omega}$ was resampled in bins, each containing n column differences or ensemble members covering an area n times larger than the OMI column spatial resolution. The resampling was performed by aggregating across-track OMI data. For $n > 60$, the number of across-track measurements, data from subsequent tracks were also used. The ensemble mean $\delta\hat{\Omega}$ was then calculated for each bin to get a set of ensemble means for each orbit. The standard

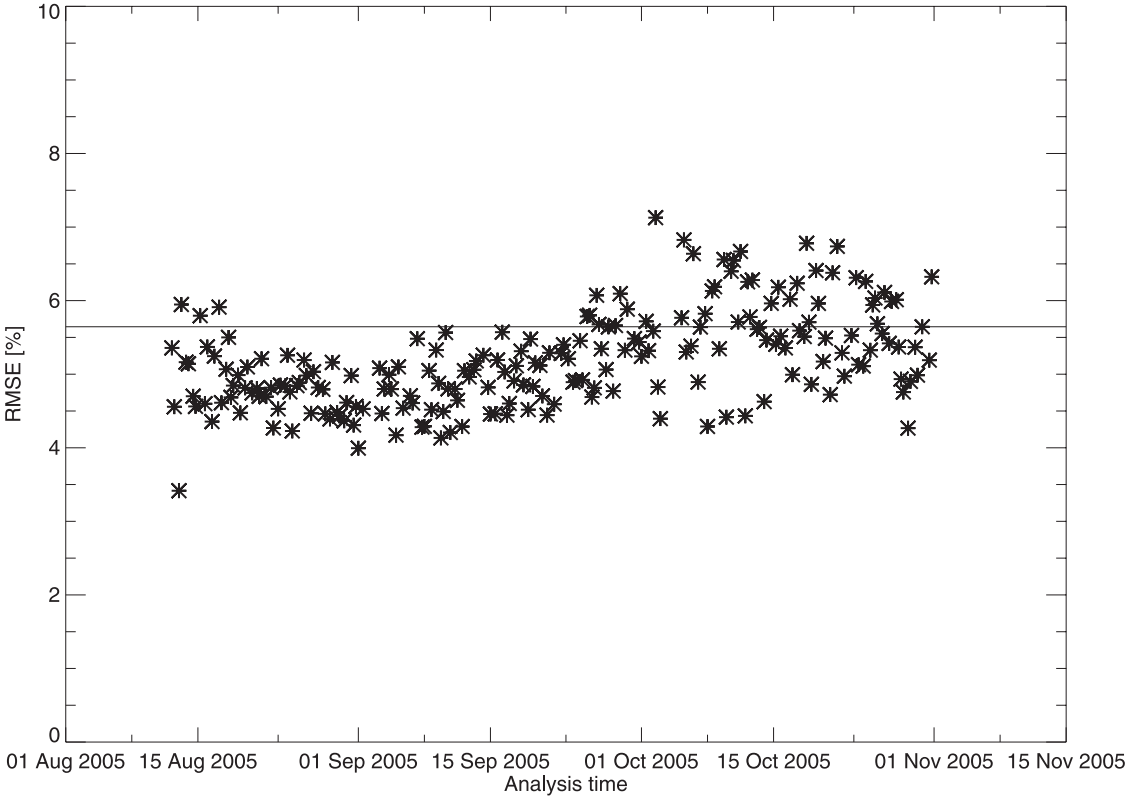

Figure 10. Time series of relative root-mean-square error (RMSE) of measured minus simulated OMI ozone total column relative differences (in %) for the 210 coincidences between 12 August and 31 October 2005. The solid horizontal line marks the value $\langle \mathrm{RMSE_{rel}} \rangle = 5.6\%$.

deviation of the set of $\overline{\delta\hat{\Omega}}$ was then computed, which is equivalent to $\sigma\left(\overline{\delta\hat{\Omega}}\right) = \sqrt{\sigma^2_{\mathrm{rnd}}/n + \sigma^2_{\mathrm{sys}}}$, the standard deviation of the mean over the n ensemble members, where $\sigma^2_{\mathrm{rnd}} \equiv \sigma^2(\epsilon_{\mathrm{rnd}})$ and $\sigma^2_{\mathrm{sys}} \equiv \sigma^2(\epsilon_{\mathrm{sys}})$. The original distribution of $\delta\hat{\Omega}$ was then resampled again and new values of $\sigma\left(\overline{\delta\hat{\Omega}}\right)$ were calculated for an increasing number n of members, from $n = 1$ up to $n = 200$, sufficiently greater than the resolution ratio between the instrument and the analyses.

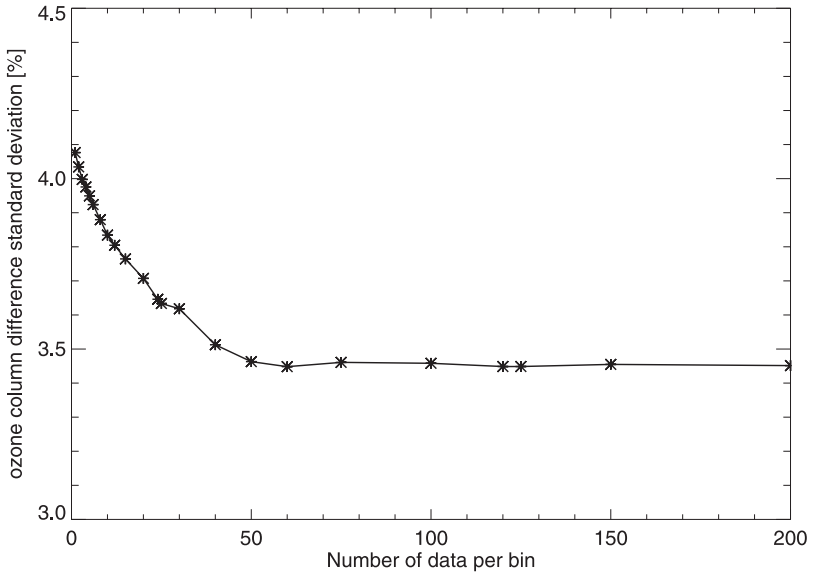

Figure 11. Standard deviation $\sigma\left(\overline{\delta\hat{\Omega}}\right)$ of the mean of n column differences per bin, as a function of n, for the OMI orbit on 15 October 2005 around 1200 UTC. Its asymptotic limit defines the value of the systematic error standard deviation according to equation (12).

Table 4. Differences Between Measured OMI Ozone Columns and Simulated Columns by Means of Ozone Analyses: Statistical Results Over the Whole Globe, for Five Latitude Bands, and for SZA < 70° During the Period 23 September to 27 October 2005[a]

	N (10^6)	$\langle\mu\rangle$ (DU)	$\langle$RMSE$\rangle$ (DU)	$\langle\mu_{rel}\rangle$ (%)	$\langle$RMSE$_{rel}\rangle$ (%)
global	7.30	−11 ± 7	15 ± 2	−4 ± 3	5.6 ± 1.2
$-90° \le \phi < -60°$	1.10	−17 ± 7	21 ± 2	−8 ± 3	9.5 ± 0.7
$-60° \le \phi < -30°$	1.36	−11 ± 7	14.6 ± 2.4	−3 ± 3	4.5 ± 1.5
$-30° \le \phi < 30°$	2.66	−6 ± 7	10.0 ± 3.6	−2 ± 3	3.6 ± 1.9
$30° \le \phi < 60°$	1.36	−13 ± 7	15.7 ± 2.3	−4 ± 3	5.3 ± 1.3
$60° \le \phi \le 90°$	0.81	−17 ± 7	20 ± 2	−6 ± 3	6.5 ± 1.0
SZA < 70°	5.86	−9 ± 7	13.0 ± 2.7	−3.2 ± 3.1	4.5 ± 1.5

[a]Here ϕ is the latitude, N is the number of differences, $\langle\mu\rangle$ is the average absolute bias, $\langle$RMSE$\rangle$ is the average root-mean-square error, $\langle\mu_{rel}\rangle$ is the average relative bias, and $\langle$RMSE$_{rel}\rangle$ is the relative root-mean-square error.

[49] Figure 11 shows $\sigma\left(\overline{\delta\hat{\Omega}}\right)$ as a function of the number of ensemble members per bin for the comparison on 15 October 2005 1200 UTC. Note that the lower limit value of the standard deviation, the systematic error standard deviation, is about 3.45%. This value is reached for n just larger than 50 which, coincidentally, is the order of magnitude of the OMTO3/analyses resolution ratio. This means that when standard deviations are calculated from ozone column differences averaged over areas that are larger than the analysis horizontal resolution, systematic error becomes the dominant error component. It also implies that the representativeness error can be taken as being at least a part if not most of the systematic error. This confirms the validity of the adopted representativeness error model discussed in section 3.1 where ϵ_R is assumed to be a systematic error. Note also that the variance decays much more slowly than $1/n$. This is likely to be due to horizontal correlations between the n analysis errors in the ensemble, as well as to correlations between retrieval errors on OMTO3 columns: the standard deviation of the mean of a set of (positively) correlated errors is greater than the standard deviation of the mean of a set of uncorrelated measurements [e.g., *Taylor*, 1997, section 9.2].

[50] Standard deviations $\sigma\left(\overline{\delta\hat{\Omega}}\right)$ as a function of n, computed for each OMI orbit in the comparison data set, are always found to spin down to a well-defined lower limit value σ_{sys} that varies in time in about the same way as the correlation coefficient time series. An average σ_{sys} value of 7.0 DU or about 3% was obtained for the period of 23 September to 27 October.

[51] By means of equations (9) and (10), it is now possible to give an estimate of the mean bias $\langle\mu\rangle$ and effective $\langle$RMSE$\rangle$, and of their errors according to equation (13) and to equation (A5) of Appendix A, over the period 23 September to 27 October. The results are $\langle\mu\rangle = -11 \pm 7$ DU or $\langle\mu_{rel}\rangle = -4 \pm 3\%$ and $\langle$RMSE$\rangle = 15 \pm 2$ DU or $\langle$RMSE$_{rel}\rangle = 5.6 \pm 1.2\%$.

[52] Finally, given that the ozone total column retrieval algorithm produces results that are latitudinally dependent (as shown by the latitudinally varying layer efficiency factors such as those in Figure 1, and by comparisons like

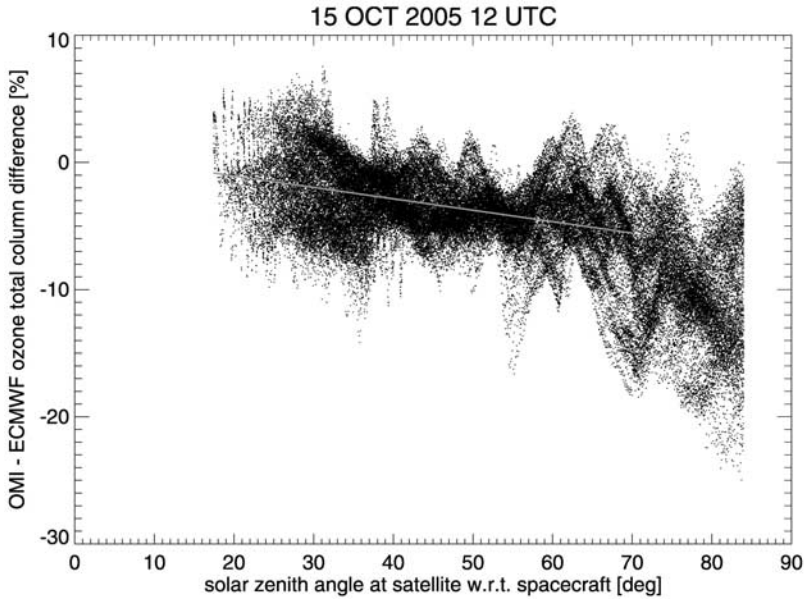

Figure 12. Measured minus simulated OMI ozone total column relative difference as a function of solar zenith angle for the coincidence valid for 15 October 2005 at 1200 UTC. The solid line shows the linear regression proposed in equation (14) for bias correction when SZA $\le$70°.

the one in Figure 8), it is possible that statistical figures related to ozone column differences may also show a similar dependence. In order to investigate such a possibility, the bias and RMSE for the total number of coincidences available were computed, with column differences subdivided in five latitudinal bands according to the location of the sub-satellite pixels. Results, summarized in Table 4, show a poorer comparison (i.e., biases and RMSE's larger in magnitude) at high and low latitudes, where OMI measurements are taken when the Sun is low on the horizon (the comparison period is around the autumn equinox, when the solar zenith angle is high near both poles). This fact may indicate that OMI estimates have systematic errors as a function of the solar zenith angle. This is discussed in the next section.

4.4. Solar Zenith Angle Dependence of OMI Ozone Estimates

[53] In Figure 12, relative differences between measured and simulated OMI ozone total columns are shown for 15 October 2005 1200 UTC. This figure clearly shows a poorer agreement for larger SZA and in particular that OMI estimates are systematically less than ECMWF analyses at large SZA. This disagreement seems to be even more pronounced for SZA > 70° when the OMTO3 algorithm makes use of an additional pair of wavelengths. A similar relationship between ozone differences and SZA is found when the same analysis is performed for a different day or time of the day within our assimilation experiments.

[54] The explanation that was first considered attributed the observed effect to an erroneous stray light correction in the 308–335 wavelength range: the OMI geophysically calibrated instrument measurement (or level-1b) data set used for retrieving OMTO3 ozone columns is known to have been calculated in this wavelength range with too much stray light subtracted [*Dobber et al.*, 2008]. However, this cannot account for the more negative values observed in the measured minus simulated OMI ozone total column difference at larger SZA given that subtracting too much stray light actually causes an increase in the OMI OMTO3 ozone total columns.

[55] A more suitable explanation for the solar zenith angle dependence is given by shortcomings in the air mass determination within the OMTO3 retrieval algorithm: errors due to the assumed or a priori distribution of ozone in the retrieval can lead to an overestimate of the relative ozone air mass, resulting in an underestimation of the ozone column that is more pronounced at high SZA [*Bernhard et al.*, 2005]. This would then limit the validity, at high SZA, of the TOMS Version 8 algorithm assumption of a linear relationship between the logarithm of the upwelling radiance and ozone and temperature increments with respect to the a priori ozone and temperature profiles selected to give a preliminary estimate of the ozone total column. This residual nonlinearity error at high SZA, usually assumed negligible for ultraviolet wavelengths longer than 310 nm [*Bhartia and Wellemeyer*, 2002], could be large enough to limit the validity of equation (2), and then the meaning of our definition of simulated OMI columns as given in equation (4). This would imply that the calculated total column averaging kernels are less reliable at high SZA. This is particularly critical given that, at high SZA in the middle stratosphere, the kernels are greater than one (see, e.g., Figure 1). According to this interpretation, the observed SZA dependence of the column differences would be mainly due to simulated OMI columns rather than to OMTO3 columns. This would be consistent with the fact that to the authors' knowledge, direct comparisons (i.e., without the use of averaging kernels) of OMTO3 data with ground based Dobson and Brewer measurements show no evidence of increased offsets near the poles.

[56] This explanation for the SZA dependence is supported by the results of the intercomparison between OMTO3 columns and simulated OMI columns obtained in the case when $\mathbf{A} \equiv \mathbf{I}$ and $\mathbf{a} = \mathbf{g}$. From equation (4), it follows that simulated OMI columns $\hat{\Omega}_{\text{ana}}$ can be expressed in this case as $\hat{\Omega}_{\text{ana}} = \mathbf{g}^T \mathbf{x}_{\text{ana}}$, and can be calculated simply by integrating ECMWF ozone profiles colocated with OMI observations, over the whole atmosphere. The above comparison was performed with the 15 October 2005 1200 UTC ECMWF ozone analysis. Results at low SZA (SZA < ∼ 40°) are found to be similar to those obtained when simulated OMI columns are defined with a realistic total column averaging kernel. This is consistent with the fact that, at low SZA, layer efficiency factors are close to one while, at high SZA, instead show evidence of a larger spread of the differences (particularly between 40° and 70°). This increased spread can be interpreted as the effect of the "smoothing" error, an additional error term given by $\mathbf{g}^T(\mathbf{I} - \mathbf{A})(\mathbf{x} - \mathbf{x}_a)$, that needs to be added at the right-hand side of equation (5) when $\hat{\Omega}_{\text{ana}}$ is defined as $\hat{\Omega}_{\text{ana}} = \mathbf{g}^T \mathbf{x}_{\text{ana}}$ and $\mathbf{A} \neq \mathbf{I}$. Also, at high SZA, no evidence is now found of a trend in SZA.

[57] Our findings suggest that our evaluation of OMTO3 columns is mainly reliable at low SZA. Therefore, part of the intercomparison of section 4.3 was repeated for OMTO3 measurements restricted to SZA lower than some threshold. Given the range of the overall linear trend in Figure 12, the threshold value was set to 70°. This threshold also corresponds to the SZA above which the OMTO3 algorithm makes use of a second wavelength pair. The results for SZA < 70° are (see also Table 4): $\langle \mu \rangle = -9 \pm 7$ DU or $\langle \mu_{\text{rel}} \rangle = -3.2 \pm 3.1\%$ and $\langle \text{RMSE} \rangle = 13.0 \pm 2.7$ DU or $\langle \text{RMSE}_{\text{rel}} \rangle = 4.5 \pm 1.5\%$. These values are slightly smaller than those provided in section 4.3.

[58] The linear trend at SZA < 70° shown in Figure 12 is unlikely to arise from the simulated columns, given that at low SZA (i.e., at SZA < ∼40°) the OMTO3 averaging kernels are equal to about one. Also, at intermediate SZA (i.e., between 40° and 70°), nonlinearity error is believed to be negligible. This trend is then likely to arise from systematic errors in the OMTO3 ozone columns. Note that the intercomparison methodology used in this work, when reliable, can reveal the presence of systematic measurement error sources better than a methodology affected by smoothing error.

[59] Our results show that it is advisable to perform a bias correction on the OMI ozone columns as a function of SZA (not higher than 70°) before using them for scientific purposes, e.g., for assimilation. This correction can be performed by means, for example, of a linear regression such as from *Dethof and Hólm* [2004, section 4]. When

such a regression is applied to our data of 15 October 2005 1200 UTC for SZA < 70° we find the following correction:

$$\hat{\Omega}^{\mathrm{BC}}_{\mathrm{OMI}} = \frac{1}{1+\frac{7.35-0.898\xi}{1000}}\hat{\Omega}_{\mathrm{OMI}} \tag{14}$$

so that, for $\xi \equiv \mathrm{SZA} > 8.18°$, the bias correction is positive and amounts to about 6% at SZA = 70°.

5. Summary and Conclusions

[60] In this paper, a comparison between OMI OMTO3 ozone columns estimated by means of the TOMS Version 8 algorithm and ozone analyses derived from assimilation of standard meteorological observations and ozone measurements from SBUV/2, SCIAMACHY and MLS into the ECMWF model was performed. Care was taken in comparing only the fraction of the total column that is actually estimated by the satellite instrument at a specific location, while accounting for the prior information present in the satellite retrievals. A procedure for estimating the standard deviation of systematic error was discussed. The estimate was then used to provide a robust estimation of the errors arising when comparing OMTO3 ozone columns to ozone analyses. Taking advantage of the large number of coincidences, it was shown that the systematic error is by far the dominant error component of the final results.

[61] The ECMWF analysis data set used for this work was compared with Brewer data over Canada. A small (less than 1% in magnitude) relative bias was found, which is likely to be partly due to a (larger in magnitude) negative bias in SCIAMACHY TOSOMI data, the largest source of ozone data assimilated into the ECMWF model for our experiment. The RMSE of the comparison at 2.8% was too large for allowing use of our analysis data set in verifying whether or not the OMI OMTO3 data can be used to extend the TOMS ozone record. However, it is small enough to make the analysis data set a valuable validation tool.

[62] A global statistical analysis of the measured minus simulated OMI ozone column data set reveals that OMTO3 data are negatively biased with respect to simulated OMTO3 data derived from ozone analyses. This leads to a global relative bias of $-4 \pm 3\%$ and a global relative RMSE value of $5.6 \pm 1.2\%$. When statistical figures are calculated for column differences grouped into latitudinal bands, a latitudinal dependence of the errors becomes evident: the bias and RMSE of the distribution of column differences is larger at higher and lower latitudes, where the satellite instrument is characterized by a low source of illumination or a high SZA.

[63] An analysis of the column differences as a function of SZA for the coincidence on 15 October 2005 12 UTC shows a negative trend with SZA. This is surprising given the absence of any evidence (to the authors' knowledge) of solar zenith angle dependence of the OMTO3 columns when compared with ground based Dobson and Brewer measurements. A possible explanation for the observed SZA trend at high SZA (i.e., at SZA $\geq 70°$) is the significant nonlinearity of the logarithm of the radiance emerging from the top of the atmosphere at 317.5 and or 312.5 nm. This makes our definition of simulated OMI ozone column less rigorous. If this explanation is correct, the trend at high SZA would be mainly due to simulated rather than measured OMI ozone columns. Results from a comparison between OMTO3 columns, retrieved from OMI measurements acquired around 15 October 2005 1200 UTC, and simulated OMTO3 columns, obtained in the case when the ozone profile averaging kernel matrix A is assumed to be equal to the identity matrix, are consistent with our explanation and show no definite SZA trend, except for SZA $< \sim 40°$.

[64] We conclude that our intercomparison needs to be restricted to columns measured at SZA lower than some threshold, set here as 70°. The observed trend at moderate SZA (i.e., at SZA < 70°) is likely to be due to systematic errors in the OMTO3 retrievals. For measurements within this SZA range, an expression for a bias correction as a function of SZA is provided. Our intercomparison results at SZA < 70° show (before any bias correction) a relative bias of $-3.2 \pm 3.1\%$ and an RMSE of $4.5 \pm 1.5\%$. Available estimates of the bias of OMTO3 columns with respect to SBUV/2 between 60° S and 60° N, as well as with respect to global Dobson data and Brewer measurements between 30° N and 60° N, are within the 1σ confidence interval of our intercomparison bias. Our statistical analysis of SCIAMACHY innovations seems to indicate that a bias correction to SCIAMACHY TOSOMI data might increase the ECMWF ozone analysis accuracy. Finally, given the relative importance of representativeness error in determining the accuracy of our intercomparison, we find that a more precise assessment of the accuracy of OMTO3 columns could be achieved by using a sufficiently higher horizontal resolution for the analyses such as T799, the current ECMWF operational configuration, corresponding to about 25 km × 25 km at the equator.

Appendix A: Uncertainty on the Estimate of the Root-Mean-Square Error

[65] Let $x_1, \ldots, x_i, \ldots, x_n$ represent a sample of independent and identically distributed normal random variables with constant mean $\mu = E\{x_i\}$, variance $\sigma^2 = E\{(x_i - \mu)^2\}$ and mean-square error (MSE) given by $\mathrm{MSE} = E\{x_i^2\}$. It can be verified that $\mathrm{MSE} = \sigma^2 + \mu^2$. Let $\hat{\mathrm{MSE}} = \Sigma_i^n x_i^2/n$ denote an estimate of the MSE, in the case when MSE is assumed to be constant. An estimate $\hat{x}$ of a constant parameter x is said to be unbiased when $E\{\hat{x}\} = x$. For the $\hat{\mathrm{MSE}}$ we have:

$$\begin{aligned} E\{\hat{\mathrm{MSE}}\} &= \frac{1}{n}E\{\sum_i^n x_i^2\} \\ &= \frac{1}{n}\sum_i^n E\{(x_i-\mu)^2\} + \mu^2 + \frac{2\mu}{n}\sum_i^n E\{(x_i-\mu)\} \\ &= \sigma^2 + \mu^2 = \mathrm{MSE} \end{aligned} \tag{A1}$$

This shows that $\hat{\mathrm{MSE}}$ is an unbiased estimator. Its variance can be calculated as

$$\mathrm{Var}\left(\hat{\mathrm{MSE}}\right) = \mathrm{Var}\left(\tilde{\sigma}^2 + 2\mu\hat{\mu} - \mu^2\right) = \mathrm{Var}\left(\tilde{\sigma}^2\right) + 4\mu^2\mathrm{Var}(\hat{\mu}) \tag{A2}$$

where $\tilde{\sigma}^2 = \Sigma_i^n (x_i - \mu)^2/n$ and where $\hat{\mu} = \Sigma_i^n x_i/n$. Note that $\hat{\mu}$ and $\tilde{\sigma}^2$ are independent random variables, being

linear and quadratic forms of multivariate normal random vectors. Since x_i is a normal random variable with mean μ and standard deviation σ, the quantity $n\tilde{\sigma}^2/\sigma^2 = \Sigma_i^n (x_i - \mu)^2/\sigma^2$ then follows a chi-square distribution with n degrees of freedom (i.e., $n\tilde{\sigma}^2/\sigma^2 \sim \chi^2(n)$). Given that $\mathrm{Var}(\chi^2(n)) = 2n$ and $\mathrm{Var}(n\tilde{\sigma}^2/\sigma^2) = n^2\,\mathrm{Var}(\tilde{\sigma}^2)/\sigma^4$, it follows

$$\mathrm{Var}\left(\hat{\mathrm{MSE}}\right) = \frac{2\sigma^4}{n} + 4\mu^2\mathrm{Var}(\hat{\mu}) = \frac{2\sigma^2(\sigma^2 + 2\mu^2)}{n} \tag{A3}$$

where $\mathrm{Var}(\hat{\mu}) = \sigma^2/n$. The root-mean-square error (RMSE) is defined as the square-root of the MSE. By using the error propagation formula it is possible to determine $\Delta\hat{\mathrm{RMSE}}$, the uncertainty on the estimate of the RMSE as

$$\Delta\hat{\mathrm{RMSE}} = \frac{\Delta\hat{\mathrm{MSE}}}{2\hat{\mathrm{RMSE}}} = \frac{\sqrt{2}}{2}\left(\sqrt{\frac{\sigma^2 + 2\mu^2}{(n-1)\hat{\sigma}^2 + n\hat{\mu}^2}}\right) \times \sigma \simeq \frac{\sqrt{2}}{2}\left(\sqrt{\frac{\hat{\sigma}^2 + 2\hat{\mu}^2}{(n-1)\hat{\sigma}^2 + n\hat{\mu}^2}}\right)\hat{\sigma} \tag{A4}$$

where $\hat{\sigma}^2 = \Sigma_i^n (x_i - \hat{\mu})^2/(n-1)$ is the unbiased estimate of σ^2 and $\hat{\mathrm{RMSE}} = \sqrt{\sum_i^n x_i^2/n} = \sqrt{\frac{n-1}{n}\hat{\sigma}^2 + \hat{\mu}^2}$, and where $\Delta\hat{\mathrm{MSE}} \equiv \sqrt{\mathrm{Var}(\hat{\mathrm{MSE}})}$. Note that in practice σ^2 has been replaced by $\hat{\sigma}^2$ with an error of the order of $1/\sqrt{n}$.

[66] Finally, when $x_1, \ldots, x_i, \ldots, x_n$ have both a random error ϵ_{rnd}, with mean μ_{rnd} and variance σ^2_{rnd}, and a systematic error ϵ_{sys}, with mean μ_{sys} and variance σ^2_{sys}, we will assume that the $\hat{\mathrm{MSE}}$ variance can be written as $\mathrm{Var}(\hat{\mathrm{MSE}}) = 2\sigma^2_{\mathrm{rnd}}\,(\sigma^2_{\mathrm{rnd}} + 2\mu^2_{\mathrm{rnd}})/n + 2\sigma^2_{\mathrm{sys}}\,(\sigma^2_{\mathrm{sys}} + 2\mu^2_{\mathrm{sys}})$. When n is large $\mathrm{Var}(\mathrm{MSE}) \simeq 2\sigma^2_{\mathrm{sys}}\,(\sigma^2_{\mathrm{sys}} + 2\mu^2_{\mathrm{sys}})$, so that we can write

$$\Delta\hat{\mathrm{RMSE}} \simeq \frac{\sqrt{2}}{2}\,\frac{\hat{\sigma}^2_{\mathrm{sys}}}{\hat{\mathrm{RMSE}}} \tag{A5}$$

where for simplicity we have assumed $\hat{\mu}_{\mathrm{sys}} \simeq 0$.

[67] **Acknowledgments.** The Dutch-Finnish built OMI instrument is part of the NASA EOS Aura satellite payload. The OMI project is managed by NIVR and KNMI in the Netherlands. We thank the OMI International Science Team for the OMI data used in this study. OMI OMTO3 and EOS-MLS O3 data were obtained from the NASA Goddard Earth Sciences (GES) Data and Information Services Center (DISC), home of the GES Distributed Active Archive Center (DAAC). SBUV/2 ozone data were obtained from NOAA/NESDIS with support from the NOAA Climate and Global Change Program Atmospheric Chemistry Element. SCIAMACHY TOSOMI data were provided by KNMI. Data from Brewer spectrophotometer instruments operated by Environment Canada were provided by the NASA Aura Validation Data Center (AVDC). This work was performed in the framework of the International ESA/KNMI/NIVR OMI "Announcement of Opportunity for Calibration and Validation of the Ozone Monitoring Instrument," providing early access to provisional OMI data sets and guidance to public OMI data. The authors would like to thank Ross Bannister, Rossana Dragani, Liang Feng, and the anonymous reviewers for their helpful comments. In particular, thanks are due to Mark Kroon (KNMI) for his encouragement and help. This work was funded by the NERC Data Assimilation Research Centre.

References

Balis, D., M. Kroon, M. E. Koukouli, E. J. Brinksma, G. Labow, J. P. Veefkind, and R. D. McPeters (2007), Validation of Ozone Monitoring Instrument total ozone column measurements using Brewer and Dobson spectrophotometer ground-based observations, *J. Geophys. Res.*, *112*, D24S46, doi:10.1029/2007JD008796.

Bernhard, G., R. D. Evans, G. J. Labow, and S. J. Oltmans (2005), Bias in Dobson total ozone measurements at high latitudes due to approximations in calculations of ozone absorption coefficients and air mass, *J. Geophys. Res.*, *110*, D10305, doi:10.1029/2004JD005559.

Bhartia, P. K., and C. W. Wellemeyer (2002), *OMI Algorithm Theoretical Basis Document, vol. 2, TOMS-V8 Total O3 Algorithm*, pp. 15–31, NASA Goddard Space Flight Cent., Greenbelt, Md. (Available at http://eospso.gsfc.nasa.gov/eos_homepage/for_scientists/atbd/docs/OMI/ATBD-OMI-02.pdf)

Bhartia, P. K., R. D. McPeters, C. L. Mateer, L. E. Flynn, and C. Wellemeyer (1996), Algorithm for the estimation of vertical ozone profiles from the backscattered ultraviolet technique, *J. Geophys. Res.*, *101*(D13), 18,793–18,806, doi:10.1029/96JD01165.

Cariolle, D., and M. Déqué (1986), Southern hemisphere medium-scale waves and total ozone disturbances in a spectral circulation model, *J. Geophys. Res.*, *91*, 10,825–10,846.

Cohn, S. E. (1997), An introduction to estimation theory, *J. Meteorol. Soc. Jpn.*, *75*, 257–288.

Daley, R. (1991), *Atmospheric Data Analysis*, Cambridge Univ. Press, Cambridge, UK.

Dee, D. P., and A. M. da Silva (1998), Data assimilation in the presence of forecast bias, *Q.J.R. Meteorol. Soc.*, *124*, 269–295.

Dethof, A., and E. V. Hólm (2004), Ozone assimilation in the ERA-40 reanalysis project, *Q.J.R. Meteorol. Soc.*, *130*, 2851–2872.

Dobber, M., Q. Kleipool, R. Dirksen, P. Levelt, G. Jaross, S. Taylor, T. Kelly, L. Flynn, G. Leppelmeier, and N. Rozemeijer (2008), Validation of Ozone Monitoring Instrument level-1b data products, *J. Geophys. Res.*, *113*, D15S06, doi:10.1029/2007JD008665.

Eskes, H. J., R. J. van der A, E. J. Brinksma, J. P. Veefkind, J. F. de Haan, and P. J. M. Valks (2005), Retrieval and validation of ozone columns derived from measurements of SCIAMACHY on Envisat, *Atmos. Chem. Phys. Discuss.*, *5*, 4429–4475.

Fioletov, V. E., J. B. Kerr, C. T. McElroy, D. I. Wardle, V. Savastiouk, and T. S. Grajnar (2005), The Brewer Reference Triad, *Geophys. Res. Lett.*, *32*, L20805, doi:10.1029/2005GL024244.

Froidevaux, L., et al. (2006), Early validation analyses of atmospheric profiles from EOS MLS on the Aura satellite, *IEEE Trans. Geosci. Remote Sens.*, *44*(5), 1106–1121.

Hilsenrath, E., R. P. Cebula, M. T. Deland, K. Laamann, S. Taylor, C. Wellemeyer, and P. K. Bhartia (1995), Calibration of the NOAA-11 Solar Backscatter Ultraviolet (SBUV/2) ozone data set from 1989 to 1993 using in-flight calibration data and SSBUV, *J. Geophys. Res.*, *100*, 1351–1366.

Jaross, G., A. J. Krueger, R. P. Cebula, C. Seftor, U. Hartman, R. Haring, and D. Burchfield (1995), Calibration and postlaunch performance of the Meteor-3/TOMS instrument, *J. Geophys. Res.*, *100*, 2985–2995.

Laprise, R. (1992), The resolution of global spectral models, *Bull. Am. Meteorol. Soc.*, *73*, 1453–1454.

Levelt, P. F., G. H. J. van den Oord, M. R. Dobber, A. Malkki, H. Visser, J. de Vries, P. Stammes, J. Lundell, and H. Saari (2006a), The Ozone Monitoring Instrument, *IEEE Trans. Geosci. Remote Sens.*, *44*(5), 1093–1101.

Levelt, P. F., E. Hilsenrath, G. W. Leppelmeier, G. H. J. van den Oord, P. K. Bhartia, J. Tamminen, J. F. de Haan, and J. P. Veefkind (2006b), Science objectives of the Ozone Monitoring Instrument, *IEEE Trans. Geosci. Remote Sens.*, *44*(5), 1199–1208.

Livesey, N. J., W. V. Snyder, W. G. Read, and P. A. Wagner (2006), Retrieval algorithms for the EOS Microwave Limb Sounder (MLS) instrument, *IEEE Trans. Geosci. Remote Sens.*, *44*(5), 1144–1155.

Migliorini, S., C. Piccolo, and C. D. Rodgers (2004), Intercomparison of direct and indirect measurements: Michelson Interferometer for Passive Atmospheric Sounding (MIPAS) versus sonde ozone profiles, *J. Geophys. Res.*, *109*, D19316, doi:10.1029/2004JD004988.

Rodgers, C. D. (2000), *Inverse Methods for Atmospheric Sounding. Theory and Practice, Ser. on Atmos., Oceanic and Planet. Phys.*, World Sci., Hackensack, N.J.

Rodgers, C. D., and B. J. Connor (2003), Intercomparison of remote sounding instruments, *J. Geophys. Res.*, *108*(D3), 4116, doi:10.1029/2002JD002299.

Schoeberl, M. R., et al. (2006), Overview of the EOS aura mission, *IEEE Trans. Geosci. Remote Sens.*, *44*(5), 1066–1074.

Stajner, I., N. Winslow, R. B. Rood, and S. Pawson (2004), Monitoring of observation errors in the assimilation of satellite ozone data, *J. Geophys. Res.*, *109*, D06309, doi:10.1029/2003JD004118.

Taylor, J. (1997), *An Introduction to Error Analysis: The Study of Uncertainties in Physical Measurements*, 2nd ed., Univ. Sci. Books, Sausalito, Calif.

Uppala, S. M., et al. (2005), The ERA-40 re-analysis, *Q.J.R. Meteorol. Soc.*, *612*, 2961–3012.

Waters, J. W., et al. (2006), The Earth observing system microwave limb sounder (EOS MLS) on the Aura Satellite, *IEEE Trans. Geosci. Remote Sens.*, *44*(5), 1075–1092.

World Meteorological Organization (2006), *An Overview of the 2005 Antarctic Ozone Hole*, *WMO Global Ozone Res. and Monitor. Proj. Rep. 49, Bull. 8*, prepared by Braathen, G. O., pp. 43–65, Geneva.

Ziemke, J. R., S. Chandra, B. N. Duncan, L. Froidevaux, P. K. Bhartia, P. F. Levelt, and J. W. Waters (2006), Tropospheric ozone determined from Aura OMI and MLS: Evaluation of measurements and comparison with the Global Modeling Initiative's Chemical Transport Model, *J. Geophys. Res.*, *111*, D19303, doi:10.1029/2006JD007089.

R. Brugge, S. Migliorini, and A. O'Neill, Data Assimilation Research Centre, University of Reading, Earley Gate, PO Box 243, Reading RG6 6BB, UK. (s.migliorini@reading.ac.uk)

M. Dobber and P. Levelt, Royal Netherlands Meteorological Institute (KNMI), P.O. Box 201, NL-3730 AE De Bilt, Netherlands.

V. Fioletov, Environment Canada, 4905 Dufferin Street, Toronto, ON, Canada M3H 5T4.

R. McPeters, NASA Goddard Space Flight Center, Code 613.3, Greenbelt, MD 20771, USA.